Chapter 8

COASTAL CIRCULATION

1 Introduction

In this chapter we consider several types of circulation that occur in coastal regions. They have distinct dynamics because of the neighboring coastal boundary and the typically strong topographic variations, and because of the buoyancy forcing by river outflows. The coastal regions also have great practical importance because they are biologically much more productive than mid-oceanic regions, with significant influence on fisheries, and because of the *water quality* (*i.e.,* chemical content) for residential, commercial, and recreational human use. For further reading, see Beardsley and Boicourt (1981), Csanady (1982), Hickey (1979), O'Brien (1975), and Tomczak and Godfrey (2003), as well as the web book by Tomczak (1998).

Tomczak (1998) lists six differences between open-oceanic and coastal circulations:

- *Effects of shallow water:* The presence of the sea floor in the $\sim$ 100s m depth-range of moderate or strong water movement is responsible for bottom-drag effects that cannot be ignored in the coastal ocean but are usually of lesser importance in deep-oceanic basins. Water movement over the sea floor establishes a boundary layer near the bottom, in the same way as wind blowing over the sea surface produces the Ekman layer through which momentum is transferred from the wind to the current. Bottom currents in the deep ocean are often so sluggish that the associated boundary layer can be disregarded in the dynamics.

- *An enhancement of tidal motion:* Tides are oceanic waves of very long wavelength and generally small amplitudes in deep water. As the tidal wave approaches the continental shelf, its amplitude increases (just as the amplitude of wind waves increases as they approach the shore through shoaling), and propagation of the wave crest is retarded. This is associated with an increase in the tidal current that in many shelf seas becomes the dominant water movement. In addition to the tidal effect evident in sea level (*i.e.,* the barotropic or external tide), an internal tide is generated when the external tidal currents move across topographic contours. The internal tide is a forced inertia-gravity wave at the tidal frequency. In some instances the internal tide can have a very large amplitude (*e.g.,* with a pycnocline displacement of $\mathcal{O}(100$ m$)$) and can propagate long distances as a solitary wave train; examples occur in the Strait of Gibraltar and Monterey Canyon.

- *The presence of coasts:* Coastlines are an obstacle to the free flow of water. A current approaching a coast will develop a horizontal convergence that results in acceleration of the flow either parallel to the coastline or downward. Where a wind produces water movement

away from the coast, the resulting surface divergence causes a rise of subsurface water to the surface, a process known as upwelling (Fig. 10). Horizontal convergences and divergences of currents are, of course, observed in deep oceanic regions as well, but they are generally much weaker, and the vertical velocities associated with them are much smaller than those produced in the vicinity of coastlines.

- *Variations in sea level produced by flow convergence and divergence due to the coast:* In the deep ocean a region of flow convergence results in sinking of water from the upper ocean to greater depth (*i.e.,* Ekman pumping) rather than any accumulation of water that elevates the sea surface. Their open ocean cannot sustain pressure gradients associated with a sloping sea surface without the assistance of geostrophic currents. In contrast, coastal seas can support strong pressure gradients without recourse to currents, since the water can "lean" against the coast., for example, by an onshore-blowing wind. This is known as a surge or — in extreme situations — a storm surge. Some shelf seas are more prone to storm surges than others, and in a few regions storm surges are among the most dangerous natural hazards (Sec. 5).

- *Stratification in shallow water:* A shallow water depth limits the volume of water available for mixing. This enhances the seasonal cycle of temperature, since the smaller water volume warms and cools faster than in the open ocean. In some shelf regions salinity undergoes strong seasonal variation, too, as a result of highly seasonal freshwater input from rain or river runoff. These forcing can lead to the establishment of a particularly strong seasonal thermocline during summer, which acts as an impediment to the exchange of properties, with reduced vertical mixing across the water column and currents restricted to the layer above the thermocline. Water quality may be adversely affected by the lack of turbulent exchange of properties, and there is an important effect of stratification on the boundary layer structure and extent.

- *Exposure to terrestrial influences:* Two of the three major elements of the hydrological cycle, evaporation and precipitation, act as sources or sinks distributed over the entire surface of the ocean. The third element, river runoff, constitutes an ensemble of point sources that exclusively impact the coastal ocean. The introduction of substantial amounts of freshwater into a shallow sea can produce horizontal density gradients large enough to support buoyancy-driven flow. The coexistence of wind-driven and buoyancy-driven flow in the upper ocean is not a situation normally encountered in the deep sea.

2 Coastal Waves and Transient Currents

The coastal region is a low-frequency waveguide (as is the equatorial region; Chap. 5) because of its side boundary which supports a coastal Kelvin wave mode and because of its cross-shore topographic slope which supports a topographic Rossby wave mode. These low-frequency wave motions are cyclonic in their propagation: poleward along eastern boundaries and equatorward along western boundaries. In addition, this wave-guide is somewhat leaky due to meridional changes in

the Coriolis frequency and some types of topographic variations, leading to a scattering of coastal waves into interior Rossby waves. Since long Rossby waves can propagate only westward, eastern boundaries are an important site of Rossby wave emission into the oceanic interior. We discuss below how this is an important process for establishing the structure of eastern boundary currents in upwelling regions.

The situation with a vertical side wall is the simplest to analyze, and we will illustrate it with an eastern boundary located at $x = 0$ in the northern hemisphere ($f > 0$). The only boundary-trapped mode is the Kelvin wave. For linear, shallow-water dynamics, a Kelvin wave has the following solution form:

$$u \;=\; 0, \quad \frac{v}{V_o} \;=\; \frac{\phi}{fRV_o} \;=\; e^{x/R}\cos\left[k(y-ct)\right], \tag{1}$$

where $c \;=\; \sqrt{g'H}\;(=\; NH) \;>\; 0$ is the speed of a gravity wave and $R \;=\; c/f$ is the deformation radius. This is a boundary-trapped, non-dispersive wave that propagates poleward along an eastern boundary. Therefore, it is a continuation of the equatorial Kelvin waveguide (Chap. 5); ***e.g.,*** signals associated with events in the tropical Pacific, including ENSO, are observed to propagate northward along the California coastline, even as far north as Alaska. During the 1997-98 ENSO event there was anomalously warm water all along the North and South American West Coasts, initiated in part by a downwelling coastal Kelvin wave from the depression of the pycnocline in the eastern Tropical Pacific. The momentum balance for (1) is a combination of along-shore gravitational accelerations and cross-shore geostrophic balance. This solution is an exact one for the f-plane approximation with linear, conservative dynamics, and it can be shown to emit Rossby waves into the interior due to $\beta \neq 0$.

The situation with a sloping bottom is more complicated because many more coastally trapped modes can occur. Figure 1 shows the dispersion relation for a semi-infinite sloping beach with upward slope α and uniform density. The eigenfrequency, ω, is a solution of the cubic equation,

$$\omega_n^2 - f^2 - \frac{fg\alpha k}{\omega_n} \;=\; (2n+1)g\alpha k\,, \tag{2}$$

which can be seen as isomorphic to the equatorial dispersion relation (***cf.,*** equation (14) of Chap. 5). For an eastern boundary the modes consist of (a) an infinite sequence of both equatorward- and poleward-propagating, high-frequency ***edge-wave modes***, whose cross-shore eigenfunction profile has n zero crossings and eigenspeed is

$$c_n \;\equiv\; \omega_n/k \;\approx\; \pm\sqrt{(2n+1)g\alpha k^{-1}}\,, \tag{3}$$

when $f^2 \;\ll\; g\alpha k$, and (b) another infinite sequence of poleward-propagating, low-frequency, rotationally-trapped boundary waves with eigenspeed

$$c_n \;\approx\; -\,\frac{f}{(2n+1)k} \tag{4}$$

in the same limit. Mode (a) obviously is a type of gravity wave. This particular coastal topography does not support an analog of the Kelvin mode, but almost any other topographic shape does.

The book by LeBlond and Mysak (1978) has a more general analysis for a variety of different cross-shore topographic shapes.

In both of these topographic situations, there are along-shore propagating waves that can be excited by along-shore wind fluctuations, especially where the fluctuation frequencies are nearly resonant. This is illustrated in Figs. 2-5 for the so-called Mid-Atlantic Bight along the U.S. East Coast. Two review articles about forced coastal waves are Allen (1980) and Brink (1991).

3 Wind-Driven Circulation

3.1 California Current System

The oceanic circulation off the U.S. West Coast is important for many human purposes including fisheries and wildlife management, prediction and abatement of pollution and toxic phytoplankton blooms, atmospheric forecasts, climate change, and shipping and military operations. The California Current System (CCS) encompasses a southward meandering current that extends up to 1000 km off-shore from Oregon to the Mexican border. It exhibits high biological productivity, rich fisheries, strong counter-currents, intricate eddy motions, and significant interannual and decadal variability.

The CCS was once thought of as a sluggish eastern boundary current driven by coastal upwelling, but satellite SST images and *in situ* and remote measurements of currents, temperature, salinity, and sea level have changed our view during the last 25 years. These observations have revealed a great variety of energetic, seasonally-dependent flow regimes with diverse characteristics. Coastal upwelling against the irregular coastline and over strongly sloping topography greatly complicates the mean-flow and eddy dynamics. Often is is even difficult to identify local mean flows in the CCS due to the high eddy kinetic energy (EKE). But recent surface-current measurements from satellite-tracked drifters clearly show a mean equatorward surface flow (Fig. 6a) and concomitant surface eddy field (Fig. 6b); the latter is also evident in fluctuations in sea-surface height (SSH) by satellite altimetry.

In Chap. 1 two situations were discussed:

- An equatorward wind stress along an eastern boundary driving coastal upwelling, with an off-shore surface Ekman current, an equatorward along-shore surface current, and a poleward along-shore sub-surface current (*i.e.,* an undercurrent). In the absence of spatial variation in the wind, the Sverdrup transport (*i.e.,* barotropic current) is zero.

- An equatorward wind stress that increases near the eastern boundary of a sub-tropical gyre has a local maximum in the anti-cyclonic wind curl, implying Ekman-pumping downwelling and an equatorward along-shore barotropic current (Sverdrup transport) that is larger than

the equatorward current in the interior of the subtropical gyre. (If, additionally, there is a decrease in the wind speed just next to the cast, then there will be a strip of cyclonic wind curl, Ekman suction, and curl-induced upwelling.)

Both of these effects occur in the quasi-steady near-surface circulation along the U.S. West Coast, as shown in Figs. 6-9.

A cartoon of this dynamical regime is shown in Fig. 10. The off-shore Ekman transport occurs within a surface boundary layer of thickness h_{bl}, with a westward velocity,

$$u_{bl} \approx \frac{\tau^y}{\rho_o f h_{bl}} < 0\,, \tag{5}$$

when $\tau^y < 0$ (*i.e.,* the climatological mean direction). Off California and Oregon, τ^y is especially strong in spring and summer. This off-shore flow is balanced by a near-shore upwelling that occurs within a region approximately R wide in the off-shore direction; hence,

$$w_{up} \approx -\frac{\tau^y}{\rho_o f R} > 0\,. \tag{6}$$

For $\tau^y = 0.1$ N m^{-2} $= \rho_o \times 10^{-4}$ m^2 s^{-2}, $f = 10^{-4}$ s^{-1}, $h_{bl} = 30$ m, and $R = 10$ km, then $u_{bl} \approx 0.03$ m s^{-1} and $w_{up} \approx 10^{-4}$ m s^{-1} $=$ 10 m day^{-1}. Note that this local rate is about 10^3 times the average upwelling rate associated with the global thermohaline circulation (Chap. 6). This is one reason for very large biological productivity in some coastal regions: deep, nutrient-rich waters are continuously brought into the euphotic zone where photosynthesis can take place. (Another reason is the large supply of nutrients from the nearby land surface, carried through both wind- and river-borne transport.)

Because of vertical advection of the stably stratified density field, the circulation in the cross-shore plane induces an upward tilt to the pycnocline approaching the shore, which can often intersect the surface in a quite sharply defined front (Sec. 7.1). It causes the near-shore water to be colder and denser (where river outflow does not counteract this by dilution; Sec. 4). We can write the cross-shore momentum balance in its thermal-wind form as

$$v_z = \frac{1}{f}\phi_{xz} = \frac{\alpha g}{f} T_x < 0. \tag{7}$$

This is a baroclinic along-shore flow, with equatorward flow at the surface and poleward flow at depth, as in Fig. 10.

The along-shore momentum balance associated with the sub-surface inflow in Fig. 10 is also geostrophic,

$$u = -\frac{1}{f}\phi_y > 0\,; \tag{8}$$

whereas the near-surface, off-shore flow is ageostrophically balanced, as in an Ekman layer, and does not induce geopotential lateral gradients. Equation (8) indicates that the sea-level, $\eta =$

$\phi(0)/g$, increases to the south. Another influence on the near-shore sea level configuration comes from the Sverdrup balance that spans the sub-tropical gyre (*i.e.,* not just within the coastal upwelling region),

$$\int dz\, v \;=\; [\rho_o \beta]^{-1} \hat{\mathbf{z}} \cdot \boldsymbol{\nabla} \boldsymbol{\tau} \;<\; 0. \tag{9}$$

This implies a southward barotropic transport and, by geostrophy, a sea-level slope down towards the coastline. Both of these slopes are evident in Fig. 7.

Along-shore currents in a coastal upwelling regime are also shown in Figs. 11-13 to illustrate three other behaviors. One is the transient onset (Fig. 11) over periods from days to seasons. After the coastal jet intensifies in response to an equatorward wind, it also begins to spread off-shore at a rate typical of baroclinic Rossby waves. This is an important influence on making the width of the California Current hundreds of kilometers, rather than the tens of kilometers for the upwelling zone. Another effect is the influence of a continental slope (Fig. 12). A strong slope can modify the shape of the undercurrent, in particular, but it does not grossly change the overall configuration of the along-shore currents. Often a more important topographic influence is the effect of its along-shore variations, especially around headlands such as Point Conception and Point Arena along the California coastline, where the coastal jet can be deflected off-shore in both transient currents (often called squirts) and semi-permanent standing meanders. This pattern is evident in Fig. 13, a map of SST on a summer day off the coast of northern California, as calculated in a regional model(ROMS) we developed at UCLA.

This map also clearly shows that there is strong eddy variability, which arises primarily from baroclinic instability of the mean along-shore currents (*n.b.,* the vertical shear between the surface current and undercurrent). Maps of surface current and SST reveal narrow energetic squirts and jets and larger-scale eddies near particular topographic features, which subsequently transport materials far away from the coast. These phenomena arise from the seasonal development of an energetic upper-oceanic mesoscale circulation forced during the summer by wind-driven coastal upwelling and the formation of an upwelling front. Upwelling centers located near coastal headlands are associated with enhanced wind-stress curl (due to orographic effects in the atmosphere) and off-shore turning of the upwelling jet. The coastal upwelling jet flows continuously through the CCS, exhibiting a coherent structure over 1000 km with peak velocities near 1 m/s. Cape Blanco (43N) appears to be the northernmost point where the equatorward upwelling jet recurrently separates from the coast, veering off-shore off the continental shelf, while deepening and gaining transport. South of Cape Blanco, the separated upwelling jet meanders through and interacts with a field of mesoscale eddies via baroclinic and barotropic instability processes (Pierce et al., 1991). At dept, a poleward undercurrent flows along the shelf break at an average depth of 200 m, a speed of 15 cm/s, and traceable continuity from 33N to 51N. A surface counter-current (the Davidson Current) also flows northward is associated with seasonal wind changes and sometimes merges with the undercurrent during surfacing events. Standing eddy flow patterns are often associated with headlands, bays, and channels (*e.g.,* Monterey Bay and the Santa Barbara Channel; see Harms and Winant (1998)). Thus, there is an important eddy-mean equilibrium circulation dynamics for the coastal regions, as well as for the basin-scale wind gyres (Chap. 3). Here too baroclinic instability

and its associated isopycnal form stress are important processes for deepening the mean circulation (Allen et al., 1991). Model solutions match the observed seasonal evolution of the surface EKE, while showing that the EKE at the surface decreases westward from the coast because of the vertical redistribution of EKE: the EKE is not strongly dissipated as it moves off-shore, rather it simply spreads downward to the deep ocean following the deepening pycnocline, resulting in a diminished surface amplitude.

Current and SSH maps from drifters and altimetry and time series from moored current meters show a region of high upper-oceanic EKE extending about 500 km off-shore. EKE has a strong seasonal cycle. Its spatial maximum occurs near the coast as part of the upwelling in early summer, then it moves westward to cover a broad off-shore region in late summer and fall (Strub et al., 1991; Kelly et al., 1998). The maximum in EKE coincides with along-shore patterns in both SST and SSH that propagate off-shore with a speed close to the expected phase speed of a baroclinic Rossby wave. However, these propagation patterns are not apparent west of about 130 W, indicating that some, as yet undetermined, process arrests, diverts, or dampens the signal. There are marked differences in vertical and horizontal scales of eddies. Near the surface they are wide (100-150 km), cold, shallow (100-150 m), and primarily cyclonic, whereas underneath they are narrow (80-100 km), warm, thick (1000 m), and more often anticyclonic (Huyer et al., 1998; Stegmann and Schwing, 2007). A theoretical interpretation that these differences are manifestations of the differing instability characteristics of the southward surface current and poleward undercurrent, although this is not entirely convincing since the two currents are in close proximity and may not be completely distinguishable in their instability behavior. Both eddy types are often highly nonlinear (*i.e.,* with a Rossby number sometimes as large as 0.5-1.0).

Satellite images and measurements from hydrographic surveys reveal great heterogeneity in the spatial and temporal distributions of chlorophyll and plankton (Denman and Abbott, 1994), hence also in the fish, mammals, and birds higher up the food chain. Recently upwelled water is stirred by mesoscale circulations, and biological distributions clearly reflect the influence of current transport, and perhaps additional intrinsic variability from ecosystem population dynamics.

3.2 Mid-Atlantic Bight

The Mid-Atlantic Bight has a mean circulation that is not so directly related to the local wind-stress driving. Figure 14 shows persistent along-shore (*i.e.,* westward and equatorward) currents at all depths, even though the prevailing wind direction is eastward and slightly poleward there. The explanation is an along-shore pressure gradient, with mean sea level decreasing by about 10 cm between, say, Cape Cod and Cape Hatteras (*i.e.,* along the flow direction). The source of this along-shore pressure gradient is not the coast circulation but rather the gyre circulations of the North Atlantic Ocean. We can represent these schematically by a double-gyre streamfunction, *e.g.,* of the form

$$\psi(x,y) \;=\; -\Psi_o(1-e^{-x/\ell})(1-x/L_x)\sin\left[2\pi y/L_y\right] \tag{10}$$

for $\Psi_o > 0, 0 \le x \le L_x, -L_y/2 \le y \le L_y/2$ and a western boundary current width $\ell \ll L_x,\, L_y$. With this circulation and the geostrophic approximation of $\phi = f\psi$, the western boundary pressure is a constant since $\psi = 0$ along the boundary. However, when $\beta L_y/f$ is not too small, as in the wind-driven gyres, the assumption of geostrophic balance is more accurately replaced by what is called *linear balance* (which is a special case of the more general, nonlinear, gradient-wind balance):

$$\nabla^2\phi \;=\; \boldsymbol{\nabla}\cdot f\boldsymbol{\nabla}\psi\,, \tag{11}$$

with a lateral boundary condition of $\phi_n \;=\; f\psi_n$. If we write

$$\phi \;=\; f\psi + \varphi, \tag{12}$$

then φ satisfies the boundary-value problem from (11),

$$\nabla^2\varphi \;=\; -\beta\psi_y, \quad \varphi_n \;=\; 0\,, \tag{13}$$

and its solution can be shown to vary along the western boundary as

$$\varphi(0,y) \;\propto\; -\beta\Psi_o \cos\left[2\pi y/L_y\right], \tag{14}$$

as sketched in Fig. 15. Thus, the sea level along the western boundary decreases towards the boundary current separation point in both the sub-tropical and sub-polar gyres. In particular, it decreases towards the Equator in the Mid-Atlantic Bight, and thus forces the mean circulation in the direction seen in Fig. 13.

Note that near both U.S. coastlines, there is an along-shore circulation directly driven by the along-shore pressure gradient against the advective "resistance" provided by $-\boldsymbol{\nabla}\cdot\overline{\mathbf{uu}}$. Along with the waveguide behavior (Sec. 2), this is yet another way that the peculiar dynamics of equatorial and coastal circulations are analogous (*cf.,* Chap. 5).

4 Buoyancy-Driven Circulation

Figure 16 is a cartoon of buoyancy-driven coastal circulations. The more common situation is an *estuarine circulation* (in the upper panel), where a river outflow injects relatively buoyant freshwater near the shore induces currents in the cross-shore plane with deep inflow, near-shore upwelling and mixing across the pycnocline (often assisted by tidal currents), and shallow outflow towards the open ocean. There are also some along-shore currents in geostrophic balance with this cross-shore density structure; however, the sense of their vertical shear is often not as well determined here as it is in Fig. 10 since both lighter and heavier waters are converging on and mixing near the shoreline. Another situation (shown in the lower panel) is often called a *reverse-estuarine circulation*, where there is a "near-shore" source of negative buoyancy, as can occur with relatively high evaporation in shallower water. The Mediterranean Sea exchanges flow with the North Atlantic Ocean through the Strait of Gibraltar in a reverse-estuarine manner.

Chesapeake Bay, near the southern end of the Mid-Atlantic Bight, has a strong estuarine circulation. Its dynamics are particularly simple since it occurs between the confining side boundaries of the Bay and thus is somewhat isolated from the other coastal circulations in the Bight. Figure 17 shows the S and σ_t (*i.e.,* $\sigma_\theta[T, S, 0 \text{ db}]$) distributions in two different cross-sections in Chesapeake Bay. Note the increase of S with depth and with distance down the Bay, which indicates the mixing between river and sea waters. Also note the isopycnal slopes that geostrophically imply an along-bay vertical shear with the expected surface outflow of an estuarine circulation (Fig. 18). Finally, note the increase in pycnocline slope, hence in circulation strength, with increasing distance down the Bay. This is associated with a continuing upwelling and entrainment across the pycnocline of the deeper water into the outflowing surface layers (as sketched in the upper panel of Fig. 16).

5 Sea-Level Set-Up and Storm Surges

Wind-generated surface currents reflect the structure of the wind field on a variety of scales. On the oceanic scale the global system of Trade Winds, Westerlies, and Polar Easterlies creates the large oceanic gyres that dominate the circulation of entire oceanic basins. On the synoptic weather scale, atmospheric low pressure systems create storms, which introduce significant variability into the oceanic current field on time scales of days to weeks. Variations of the wind field in space generate convergences and divergences of the oceanic flow field on all scales.

In principle, a region of surface flow convergence means an accumulation of water in the convergence region. However, in the open ocean such accumulation is kept small, because a rise of the sea level from accumulation of mass immediately causes a depression of the thermocline, followed by vertical water movement from the upper ocean to greater depth. The main effect of a surface convergence is thus vertical exchange of water between the upper ocean and the underlying regions by Ekman pumping. Variations of sea level in the open ocean are therefore modest, of the order of tens of centimeters, and rarely reach 1 m in height. In the coastal ocean the situation is quite different. To begin with, currents in the open ocean rarely oppose each other on scales of tens of kilometers, and convergences (or divergences) are usually the result of slow changes in current speed and direction. The presence of a coast inhibits horizontal water flow and produces vastly stronger convergence (and divergence) effects than are ever encountered in the open ocean. Another factor is the restricted water depth on the shelf. The depth of the coastal zone usually does not exceed 200 m or so, which poses a severe restriction on vertical water movement on a large scale. As a result, water can pile up against the coast to great height, a phenomenon known as sea level set-up or surge. Sea level set-up can pose a severe threat to coastal land and can lead to large scale flooding and loss of life in low lying coastal regions.

The major cause of sea level set-up is atmospheric storm systems. Stronger storms are of course more dangerous than moderate storms; but the severity of the resulting storm surges depends on the coastal topography just as much as on the absolute wind strength. When water is piled up

Table 1: Historical Storm Surges

Place	Date	Height	Lives Lost
Zuider Zee (Dutch North Sea)	1218	unknown	100,000
India and Bangladesh	1737	12 m	300,000
Bangladesh	1876	15 m	100,000
Galveston, Texas	1900	4.5 m	6,000
Southern North Sea	1953	3.0 m	2,000
Bangladesh	1970	9.0 m	500,000

against a coast, the sea surface slope has the momentum balance,

$$\frac{\partial \eta}{\partial x} = \frac{\tau}{\rho g H},$$

where H is the local water depth. Some parts of the world's shelf regions are more susceptible to storm surges than others. Figure 19 shows an example of a storm surge in the North Sea. The storm system responsible for a surge in the North Sea is usually generated in the region of the Westerlies over the North Atlantic Ocean. It moves with the westerly wind in a generally north eastward direction, passing north of Scotland and continuing along the Norwegian coast. The storm produces a weak surface elevation anomaly in the open ocean that induces flow entering the North Sea from the north and builds up in height as it crosses the continental slope and enters shallower water. Under the influence of the Coriolis force, which in the northern hemisphere acts to the right of the movement, the surge leans against the British coast and increases in height as it moves south towards the Dutch and German coast.

The severity of a storm surge depends to a large extent on its timing relative to the tidal cycle. Many storm systems pass quickly and produce a surge of not much more than 12 hours in duration. If the peak of the surge occurs at low tide, the effect will be minimal. If, on the other hand, the peak of the surge coincides with high tide, the water level can reach quite unusual height. The most dangerous storm surges are produced by long lasting storm systems that coincide with spring tides. There have been surges during which the water level did not fall after high tide but kept rising despite of ebb tide, bringing the following high tide close to the height of the dykes along the coastline. The constant pounding from the sea under the lashing of the storm is a severe test for any dyke system. A lot of land can be flooded when a dyke breaks, the force of the water rushing in is quite destructive.

Some examples of especially damaging and deadly storm surges are listed in Table 1. This list indicates that the North Sea and the Bay of Bengal are highly exposed to severe storm surges, particularly the coastline of Bangladesh where the nearby land is low-lying. Whether a storm surge develops into a human disaster is determined by several factors. The Netherlands is one of the most densely populated countries of the world. Most of the country is below sea level and

relies on dykes keeping the sea out. It experiences severe storm surges every year but is very rarely flooded because an infrastructure built over centuries and maintained by a rich nation to secure the coastline. The disproportionate number of casualties in Bangladesh is exacerbated by the country's under-development and poor emergency response capability. The coastal defenses of Bangladesh are of ancient design and the country lacks the resources to improve and maintain them. Another factor that turns Bangladesh's storm surges into national calamities is its close proximity to the equator, allowing typhoons (called hurricanes in the Atlantic) where the wind and rain are very much more powerful than in the storm systems experienced in the North Sea. Typhoons and hurricanes can produce intense surges, with the sea level sometimes rising by several meters in a few hours.

6 External Tides in Shallow Seas

OGCMs (Chap. 7) are constructed without including tidal forcing, and even mixing parameterizations explicitly related to tides are relatively rarely used. The presumption is that the tide is a low-amplitude periodic motion and does not contribute to the balance of forces for the steady state. The situation is different in shallow seas, even if we consider only the steady state. In many shallow seas tidal movements, though still periodic, are not weak, and they can result in a mean water movement known as the residual flow or *tidal rectification*: a tidally-averaged current driven by the Reynolds stress of oscillatory tidal motions due to spatial inhomogeneity induced by their flow over topography. In some locations with strong tides and topography, the rectification currents can be 0.1 m s^{-1} or more, *e.g.,* over the Georges Bank (Chen et al., 1995). Furthermore, tidal currents cause mixing strong enough to determine the stratification in some shallow seas. Estuarine dynamics depend heavily on the tides, and even the mean circulation often cannot be understood without their effects.

The astronomical, tide-generating, gravitational force is on a global scale. However, only the largest water bodies such as the major oceans respond to tidal forcing directly (*i.e.,* in the way described by Laplace; Longuet-Higgins (1968)). Smaller water bodies such as marginal seas or estuaries are less significantly responsive directly to the astronomical forcing than they are by the tidal currents from the deep ocean that enter and leave the region periodically at the connection to the ocean. Tides generated in this way are known as co-oscillation tides. Marginal seas have their own resonance frequencies, determined again by their shape and size. As a consequence, the amplitudes and phases of co-oscillation tides depend on the nearness of a resonance frequency to one of the tidal frequencies and on the amplitude of the tidal currents in the deep ocean at the connecting line with the marginal sea. This explains, for example, why some enclosed seas are virtually tide-free; the connection with the open ocean is so restricted that the oceanic tides cannot produce co-oscillation. The largest tidal range occurs in the Bay of Fundy on the Canadian Atlantic coast. This bay is 150 km long and 30 km wide and at spring tide experiences a tidal range of 21 m. The North West Shelf of Australia is another region with large tidal resonance; the tidal range on the North West Shelf reaches 8 m and more.

A large tidal range is of course always associated with strong tidal currents, and tidal currents on the shelf are always larger than tidal currents in the open ocean. In some locations tidal currents can become unusually strong even under a moderate or small tidal range. This occurs where constrictions prevent the free flow of the tidal wave and force it to rush through narrow openings. The most spectacular tidal current of this type is the famous"maelstrom" in the Saltfjord of northern Norway. This 500 m deep fjord is connected with the North Atlantic Ocean by a 3 km long channel of only 150 m width and 31 m depth. The channel is much too small to allow the fjord to follow the oceanic tide, and the difference in water level between the two ends of the channel can reach up to 1 m. This produces a periodic current through the channel of speeds in excess of 20 knots (up to 40 km/h) which produces intense whirlpools (maelstroms) of 10 - 15 m diameter. Calm conditions every 6 hours allow ships to pass through the channel, before the current starts again. A coastal inlet in the Kimberleys of Western Australia shows even stronger tidal currents. Its connection to the North West Shelf is only a few hundred meters long and barely 50 m wide. The difference in water level on either side of the connection is clearly visible from the top of the cliff, as a tidal waterfall (*i.e.,* bore) rushes through the gap, changing direction every six hours.

Shallow seas that are close to resonance with one of the tidal periods are of great importance for the world's fishing industry. The flow of strong tidal currents over a shallow oceanic floor produces turbulence of sufficient intensity to keep the entire water column well mixed throughout most of the year. Nutrients which usually accumulate in the sediment and are no longer available to support marine life, are continuously kept in suspension under such conditions. These coastal seas are therefore among the most productive fishing regions of the world ocean, rivaling the great coastal upwelling regions and the fertile Southern Ocean with planetary-scale upwelling (Chap. 4). The North Sea and the Grand Banks off Newfoundland are examples of regions where tidal mixing keeps nutrient concentrations in the water column at a high level.

Tides in shallow water are generally a mixture of propagating waves and standing waves. For a given coastal location the time of strongest tidal current relative to high tide therefore depends on the type of tidal wave in the region.

7 Surface Fronts

Fronts in the ocean or in the atmosphere can be defined as regions where properties change markedly over a relatively short distance. How short this distance is depends on the scale of the process responsible for the front's existence. Semi-permanent fronts in the open ocean (also called planetary fronts) can reach 100 km in width; fronts near the coastline or in estuaries may only be a few meters wide. What both have in common is the change of some hydrographic property — temperature, salinity, *etc.*— across the width of the front an order of magnitude larger than changes of the same property over a similar same distance on either side of or along the front. Thus, fronts are zones where the horizontal gradient of a property has a significant maximum.

One frontal type is sometimes called a *planetary front*. It is restricted to the open ocean and is usually associated with the large-scale wind pattern. Such fronts are sometimes density-compensated (*i.e.,* $\alpha\Delta T \approx \beta\Delta S$) with a high degree of interleaving of the adjacent water masses. A typical example is the Subtropical Front which is formed by convergence in the Ekman layer flows at the boundary between tropical Easterlies and extratropical Westerlies. Other planetary fronts are found in the ACC and between the subtropical and subpolar oceanic gyres of the northern hemisphere. In comparison, fronts in the coastal ocean are generally smaller in extent and often less permanent in existence than fronts of planetary scale.

An important dynamical distinction for fronts is whether the frontogenesis is due to convergent or confluent horizontal flow at the surface. Convergent flow, *e.g.,* along the x axis, is locally expressed as

$$u \;=\; -\delta x\,, \quad v \;=\; 0\,, \quad w \;=\; \delta z\,. \tag{15}$$

With $\delta > 0$ this flow brings surface material towards $x = 0$ and carries it downward into the interior (where $z < 0$). If there is initially a tracer gradient in x, it will be sharpened in x by advection, and the resulting tracer front will become increasingly aligned with the y axis. This type of frontogenesis is illustrated in Fig. 20. If, for example, the front is the boundary between cold and warm water, flow convergence advects cold water from the cold side and warm water from the warm side. The resulting increase in the thermal gradient across the front is large enough to overcome any effect of mixing. By geostrophic balance, there is an associated surface-intensified flow along the frontal axis. Because temperature and salinity, the most frequently measured hydrographic properties, determine the stability of the water column, they often are not good indicators for vertical water movement. Downward movement in the frontal zone is, however, clearly seen in passively-advected optical properties. Figure 21 demonstrates this with observations of fluorescence in a frontal region of the western Mediterranean Sea.

Confluent flow also has the advective effect of sharpening tracer gradients in x to create a front aligned with the y axis. It is expressed as

$$u \;=\; -\alpha x\,, \quad v \;=\; \alpha y\,, \quad w \;=\; 0 \quad [\alpha > 0]\,. \tag{16}$$

This flow and its resulting front are sketched in Fig. 22. Because most large- and mesoscale flows in the ocean are approximately geostrophic and horizontally non-divergent, the typical magnitude of α (also called the horizontal strain rate) is larger than the horizontal convergence rate δ. Furthermore, mesoscale values of α are typically larger than planetary-scale values. So mesoscale confluence is perhaps the more common cause of oceanic frontogenesis (*e.g.,* as in Fig. 23), although shallow coastal regions also frequently have convergent flows.

Insofar as there is frontogenetic flow across quasi-stationary isopycnal or other material surfaces in fronts, there must be significant local mixing. Fronts are also susceptible to instabilities, especially after the frontogenetic flow abates. Examples of frontal instability in the California Current are in Fig. 23. The California Current System (*cf.,* Fig. 13) has abundant submesoscale fronts during the active upwelling seasons (Catelao et al., 2006), even off-shore of the active upwelling zone with its characteristic upwelling front (Sec. 7.1).

Managing the coastal ocean requires an understanding of frontal dynamics for various reasons. Floating material accumulates in fronts, a result of the flow convergence at the surface. This is an important consideration in strategies to combat pollution from oil spills since the buoyant oil slick will be trapped in the front. Search and rescue operations have to account for the presence of fronts since a drifting stricken small craft will remain in a front even when exposed to considerable wind, particularly when it is partly filled with water and nearly completely submerged. Detritus and particulate matter also accumulate in fronts, and if pollutants such as heavy metals can attach to this material, their concentration will be higher in the fronts than in the surrounding sea, often by orders of magnitude. The same effect is responsible for the concentration of nutrients in frontal regions, which can form the basis for increased primary production and makes larger fronts in particular attractive feeding grounds for fish. Tuna are among the species that tend to congregate in frontal regions, and the tuna fishery regularly uses satellite derived SST maps to identify potential fishing grounds.

7.1 Upwelling Fronts

We begin our discussion of fronts in the coastal ocean with the upwelling front, an elementary ingredient of coastal upwelling systems already discussed (Sec. 3.1). The upwelling front forms when the thermocline breaks the surface as a result of upward water movement in the coastal boundary layer. It is embedded in the general off-shore movement of the Ekman layer, and its location on the shelf follows the strengthening and weakening of the upwelling circulation. The strength of the upwelling is determined by the strength and direction of the wind. Most important upwelling regions are located in the Trade Wind region where winds are relatively uniform in strength and direction. But the atmospheric circulation contains instabilities, depressions which bring a temporary increase in wind speed as they pass through. These depressions are most prominent in the wind systems of temperate regions but exist in the Trade Wind region as well. They cause periods of intense upwelling, so-called upwelling events that alternate with periods of weak upwelling.

The duration of an upwelling event and the following lull in the upwelling is typically one to two weeks. This cycle dominates the movement of the upwelling front, which is seen to move in and out from the coast with the same period. In a way the upwelling front is the most visible expression of variability in the upwelling system, since it is constantly shifting its position in response to the wind. Like all other fronts it is associated with a surface convergence, which causes surface water to sink in the frontal zone. This was clearly borne out during an experiment to study primary productivity in the Canary Current upwelling region, in which a drifting buoy was used to follow freshly upwelled water. The buoy invariably drifted towards the front, reached it within a few days, and then stayed trapped in it for several more days. The upwelling front therefore constitutes the seaward limit of the active upwelling region. The presence of this surface convergence on the outer shelf is important for the upwelling ecosystem since it prevents passive substances such as phytoplankton from drifting out to sea and keeps it in the region of high primary

production on the shelf. Slow swimmers such as zooplankton also find assistance in their attempts to stay within the region of high productivity.

Density fronts in the coastal ocean are sometimes distinguished according to the slope of their isopycnals. A density front in which the isopycnals slope upward towards the coast is known as prograde; a density front in which the isopycnals slope downward towards the coast is called retrograde (Fig. 24). In a prograde situation the shelf water is denser than the water on the seaward side of the front; in a retrograde situation it is less dense. Upwelling fronts are always prograde fronts.

7.2 Shelf-Break Fronts

Shelf-break fronts are the result of differences in hydrographic properties between the coastal ocean and the open sea. The ocean's response to atmospheric forcing is modified in the coastal ocean through limited water depth and freshwater input from point sources along the coast. The water of the coastal ocean can therefore be significantly fresher, saltier, colder or warmer than the water of the adjacent deep ocean, effectively constituting a different water mass. A horizontal pressure gradient is established where the two water masses meet. Acting on its own, it would establish a two layer circulation, with water from the open ocean invading the shelf and shelf water escaping into the open ocean. Given the rotation of the earth, it becomes part of a geostrophic balance that establishes flow along the isobars rather than across. In other words, the open-oceanic water does not invade the shelf but moves geostrophically along its outer edge. This defines the seaward limit of the shelf as the location for the boundary between shelf water and open-oceanic water at or near the shelf-break.

This brief discussion of the dynamics of shelf-break fronts is sufficient to bring out a major distinction between shelf-break fronts and other fronts of the coastal ocean. In contrast to upwelling fronts and shallow sea fronts, shelf-break fronts are more or less stationary; their mean position is entirely controlled by the location of the shelf break. Departures from this position are observed only during eddy formation. The difference between the hydrographic properties on the shelf and in the adjacent deep ocean is responsible for its existence but does not influence its position.

Shelf-break fronts can be density fronts or density-compensated fronts. Most shelf-break fronts display some degree of density compensation but still support a horizontal density gradient, which makes their classification ambiguous. Theory shows that if the density difference is strong enough to prohibit significant interleaving across the front, it determines the width of the frontal zone, which is approximately the baroclinic deformation radius, R, with a typical coastal scale of 10-20 km.

A shelf-break front is not an impenetrable barrier for shelf and oceanic waters. If, as in the case of Fig. 25, the shelf water is less dense than the water of the oceanic surface layer, mixing in the frontal zone will transfer some of it into the ocean. If the shelf water is denser, it will eventually

make its way down the continental slope to the depth where the oceanic water matches its own density and spreads into the interior on this density surface. An example for this process is in the Bass Strait, a shallow region between Tasmania and mainland Australia. Bass Strait is bowl-shaped with a maximum depth of 80 m in its center and sill depths of 55 m on its western and 75 m on its eastern side. The seasonal thermocline in the adjacent Tasman Sea is located deeper than the sill depth, and as a result the waters of Bass Strait get about 2^oC colder in winter than the water in the surface layer of the Tasman Sea. This produces a shelf-break front along the eastern edge of Bass Strait. A small salinity difference between Bass Strait and the Tasman Sea is not large enough to compensate the density effect of the temperature difference, and Bass Strait water is denser than Tasman Sea surface water by about 0.4 in σ_t units (*i.e.,* $10^{-3}(\rho - \rho_0)$).

7.3 Shallow-Sea Fronts

The last type of front found in the coastal ocean is known as a shallow-sea front (probably the best studied and understood of all fronts). It occurs in shallow regions with moderate to strong tidal currents and is the result of competition between two energy inputs into the ocean. Heat input from solar radiation tends to establish a stratification in the water column. Tidal currents flowing over the sea floor produce turbulent mixing that tends to suppress or destroy stratification. A coastal sea will be stratified where the mixing effect of the tidal current is insufficient to break down the stratification caused by the heating at the surface; it will be totally mixed where the tidal mixing is strong. The boundary between the two regions is marked by a shallow-sea front.

It is possible to predict the occurrence and location of shallow-sea fronts through an analysis of heat input and tidal current. Heat input is greatest in summer and least in winter (when, in temperate and subpolar climates, it turns into heat loss). Tidal currents are weak in the deep ocean but increase in magnitude as the tidal wave enters shallow water. As one approaches the coastal sea from the deep ocean there comes a point where the stratification found in the deep sea can no longer be maintained against the increasingly vigorous tidal mixing. The situation is shown schematically in Fig. 26. The front is associated with a density gradient and thus supports a geostrophic jet along it, which causes eddies to form and break off. Like all other fronts it is also linked with a convergence of the surface current.

Since the temperature in the homogeneous region is the result of mixing the water column from the surface to the bottom, it is colder than the surface temperature in the stratified region but warmer than the temperature in the layer below. It therefore corresponds to the temperature found somewhere in the center of the thermocline. This unique feature of shallow-sea fronts helps in their identification.

Theoretical analysis of the balance between heat input and tidal mixing shows that the location of shallow-sea fronts is determined by the ratio H/u^3, where H is water depth and u the tidal current amplitude (the maximum tidal current during one tidal period). Shallow sea fronts are therefore also known as H/u^3 fronts. Comparison with observations demonstrates that the critical

value for the transition from stratified to mixed (*i.e.,* the location of the front) is somewhere near $\log_{10}(H/u^3) = 2.5$ or so. It is thus possible to predict the existence of shallow-sea fronts from a knowledge of water depth and tidal current. The dependence of the frontal location on the magnitude of the tidal current can lead to regular movement of the front. If the tides have a pronounced fortnightly inequality (there is a marked difference between spring tides and neap tides), the frontal location moves off-shore during spring tide and retreats into shallower water during the neap tide. Shallow-sea fronts have been shown to be regions of strongly-enhanced, biological primary production.

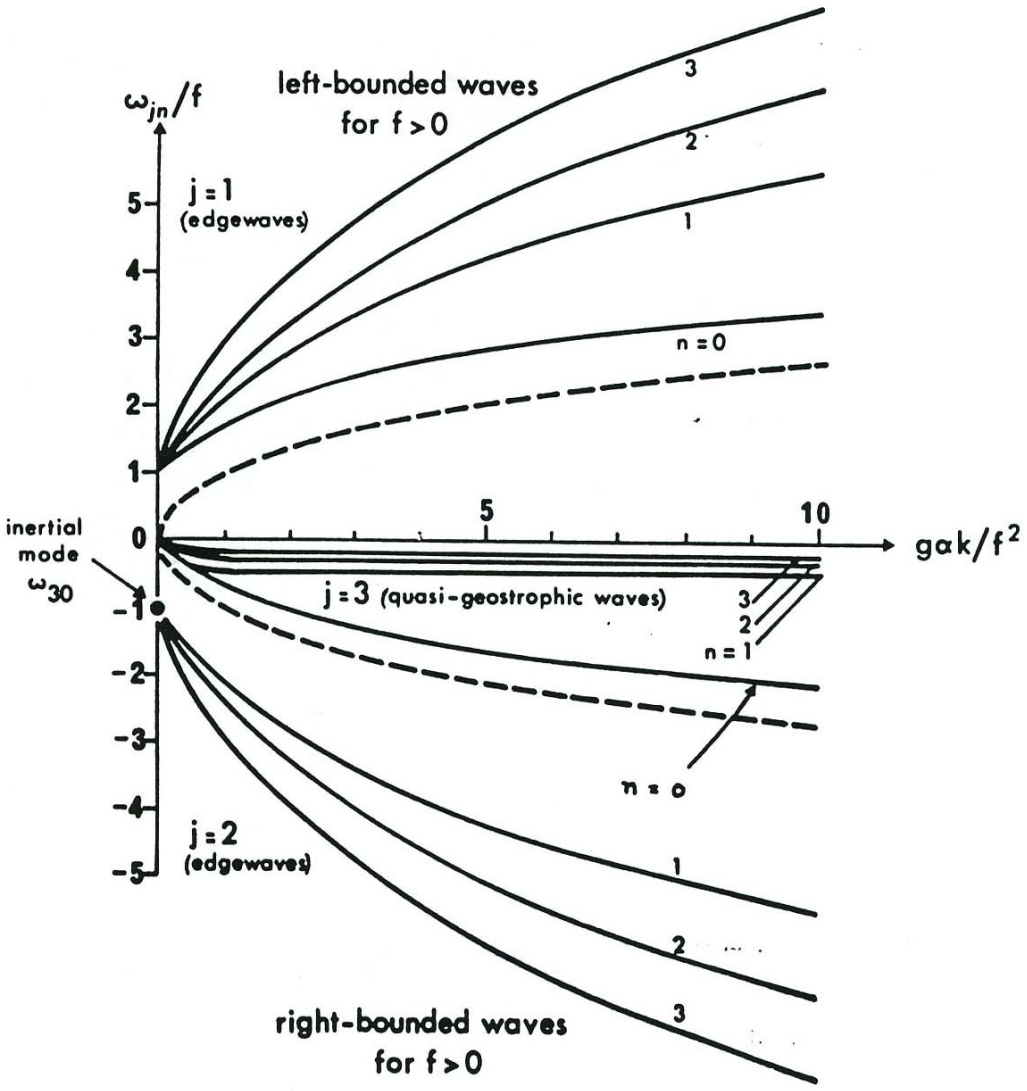

Figure 1: Dispersion relation for waves on a sloping beach (LeBlond and Mysak, 1978).

dfigure

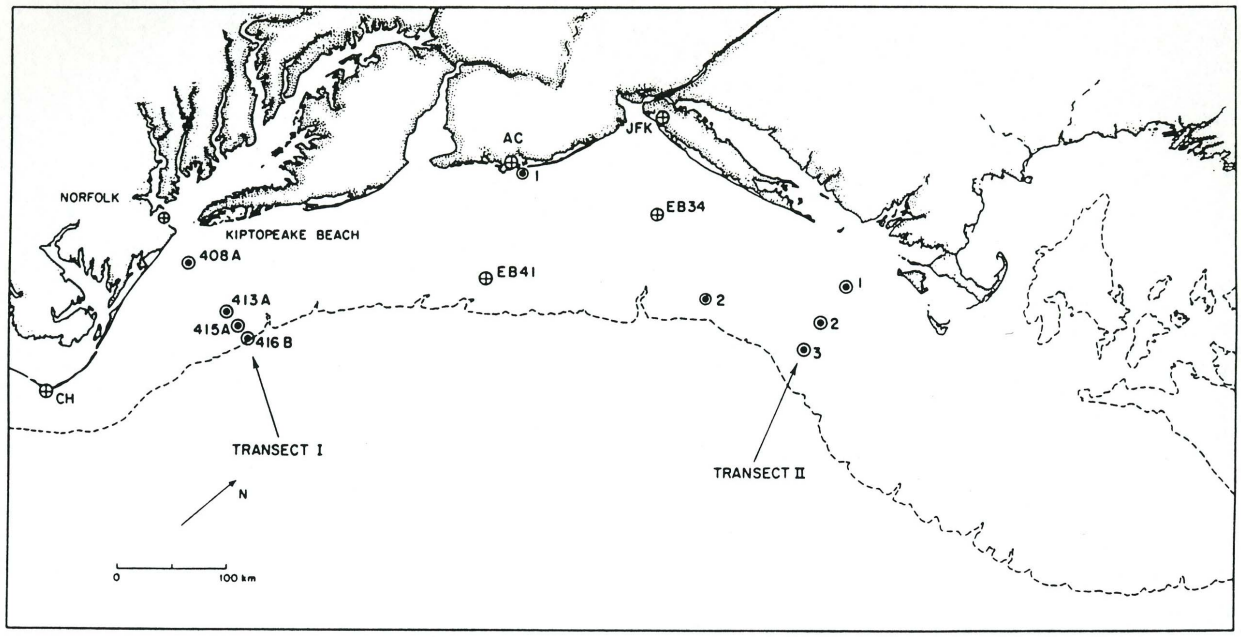

Figure 2: The Mid-Atlantic Bight (Beardsley and Boicourt, 1981).

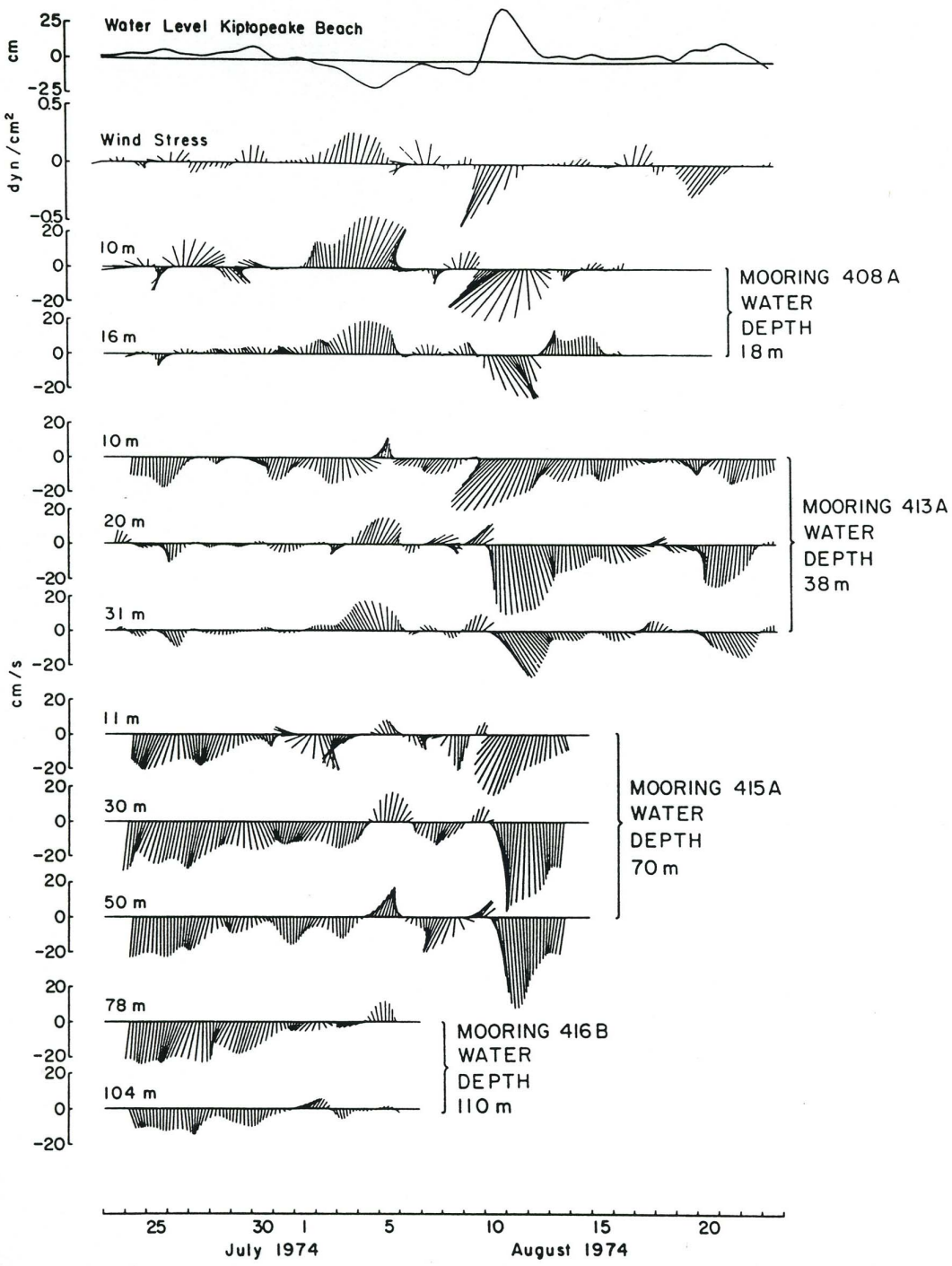

Figure 3: Summer currents in the Mid-Atlantic Bight (Beardsley and Boicourt, 1981).

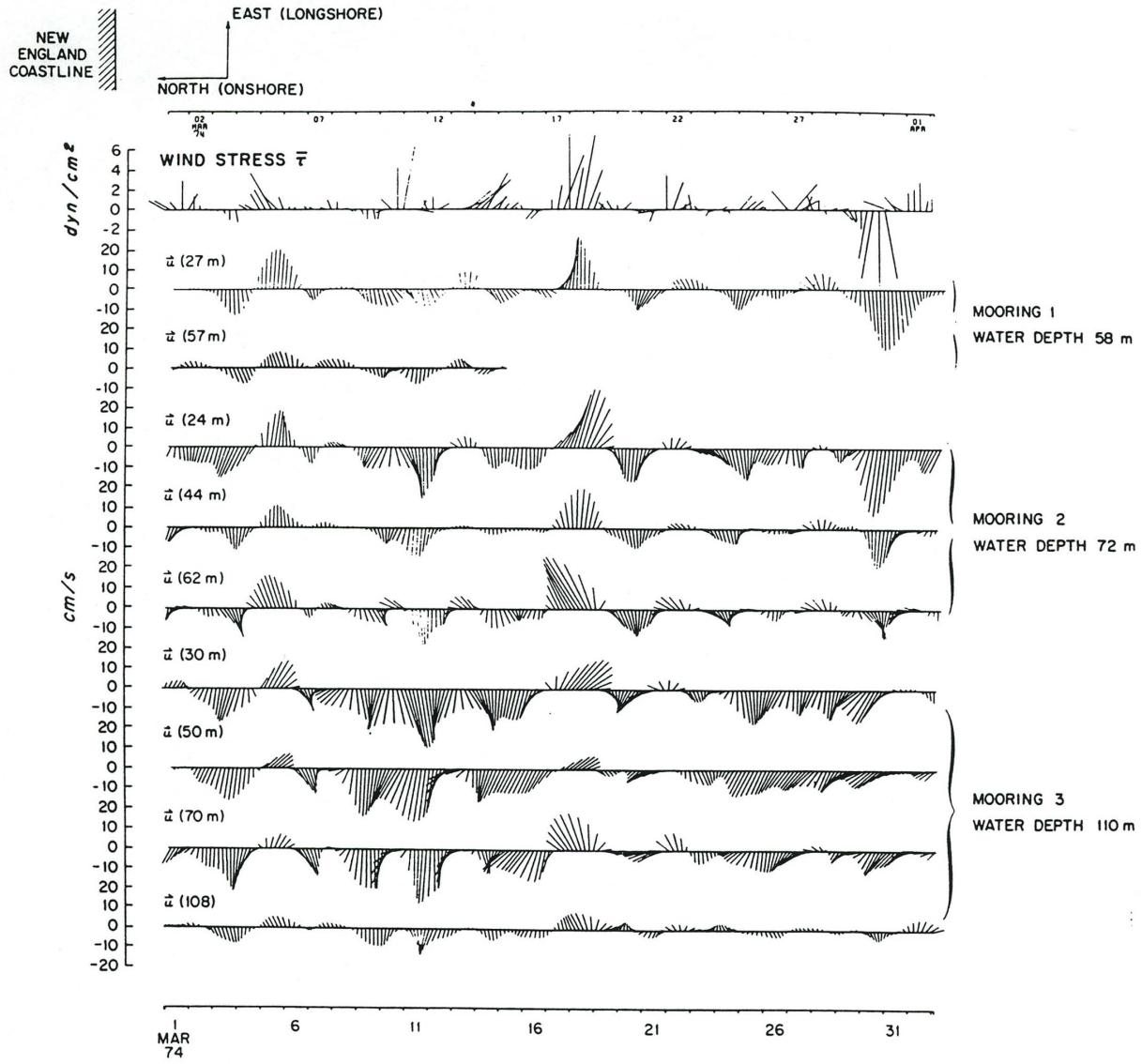

Figure 4: Winter currents in the Mid-Atlantic Bight (Beardsley and Boicourt, 1981).

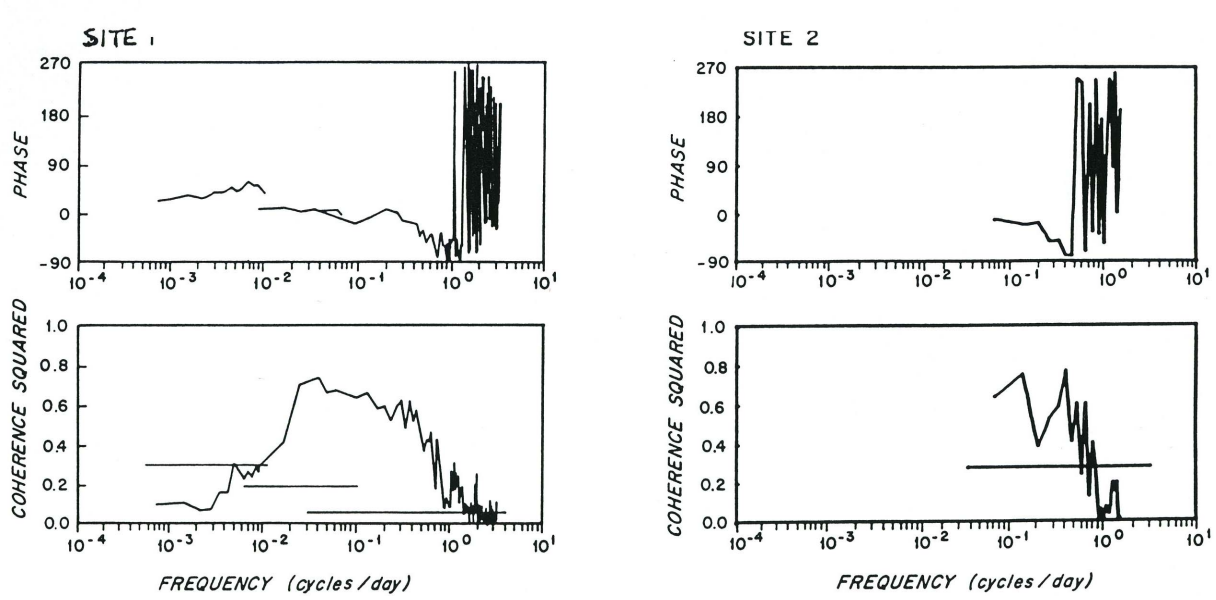

Figure 5: Coherence analysis between winds and currents at two sites in the Mid-Atlantic Bight (Beardsley and Boicourt, 1981).

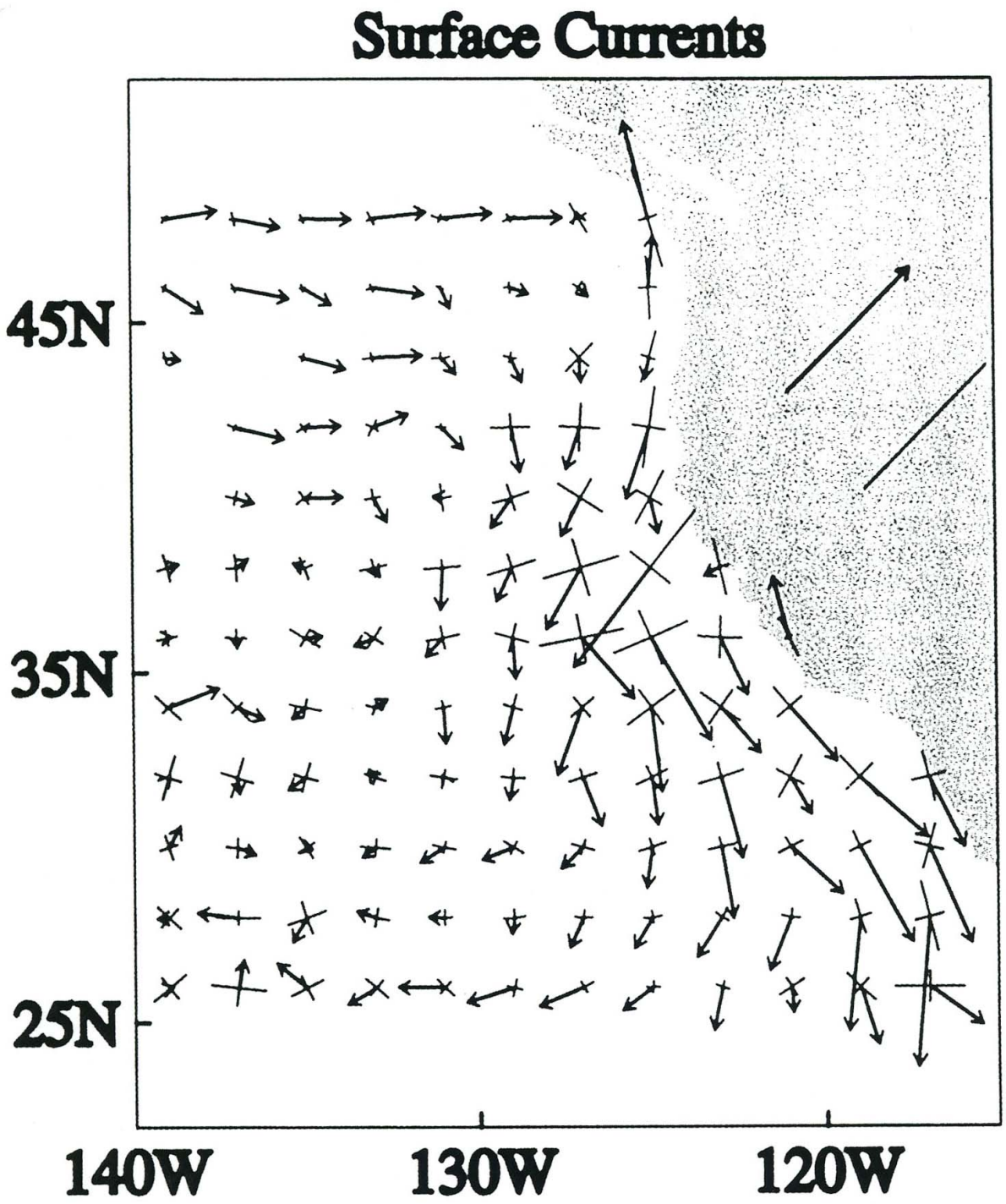

Figure 6: (a) Mean 15-m velocity (cm/s) and (b) its variance (cm^2/s^2) in the CCS and eastern Pacific from available surface drifters during the period 1985-98 (Swenson and Niiler, 1996).

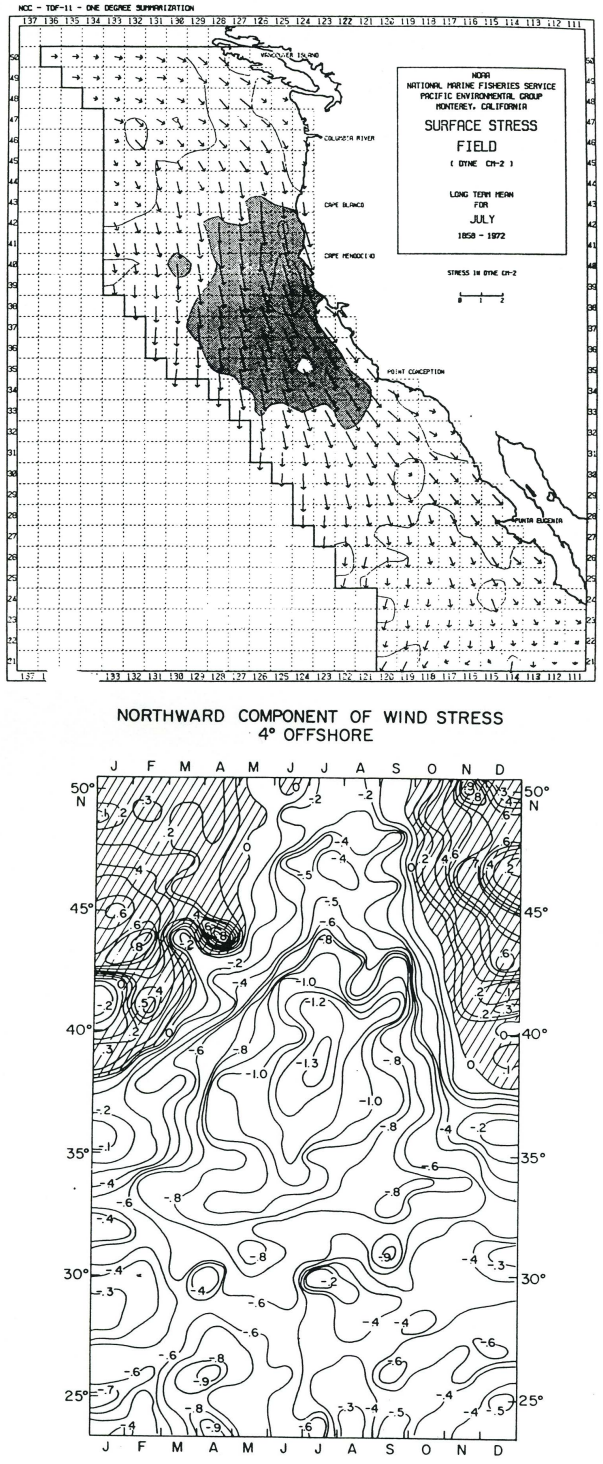

Figure 7: (a) Summer winds and (b) seasonal cycle of winds off the U.S. West Coast (Hickey, 1979).

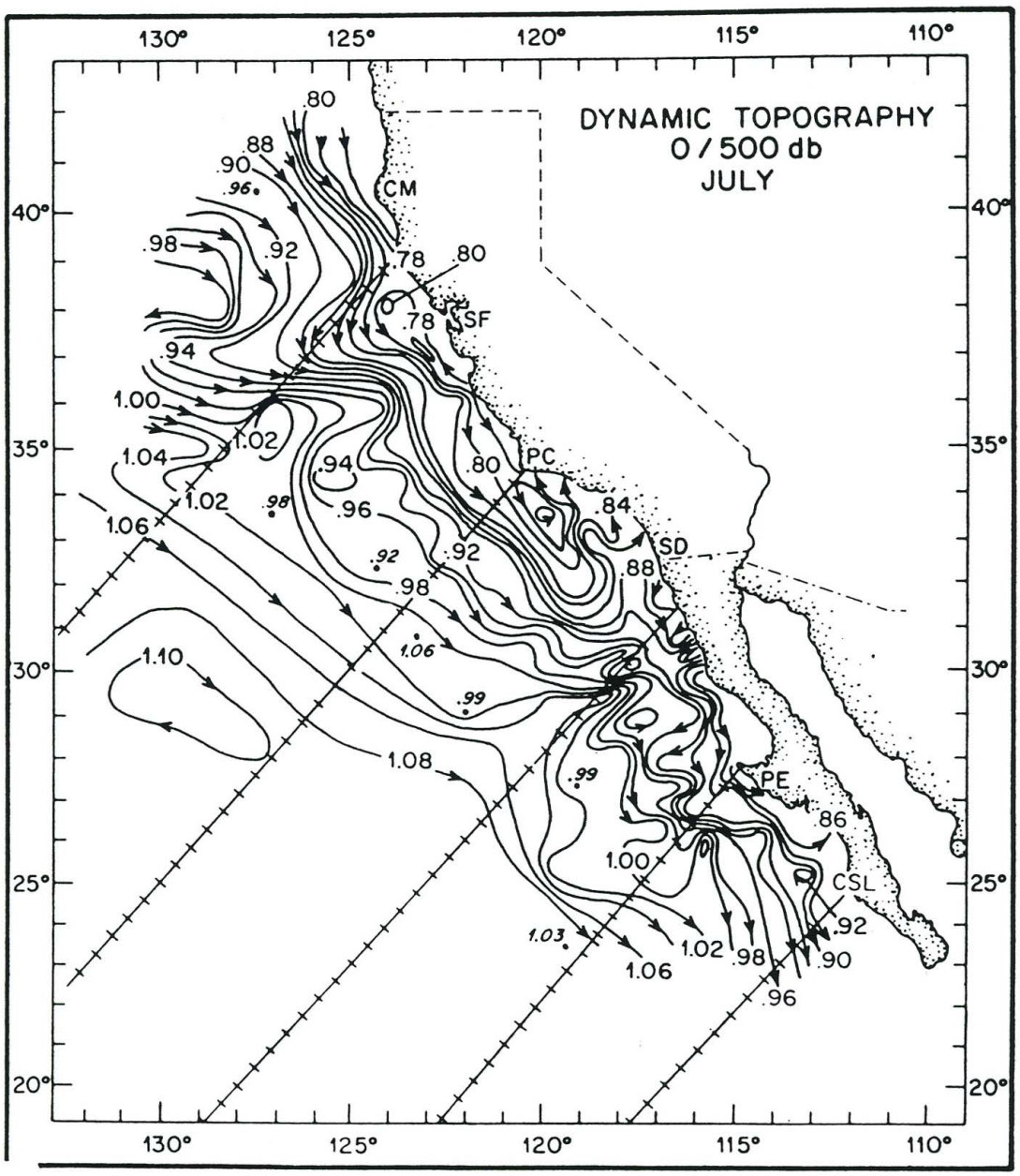

Figure 8: Annual-mean surface dynamic topography off the U.S. West Coast (Hickey, 1979).

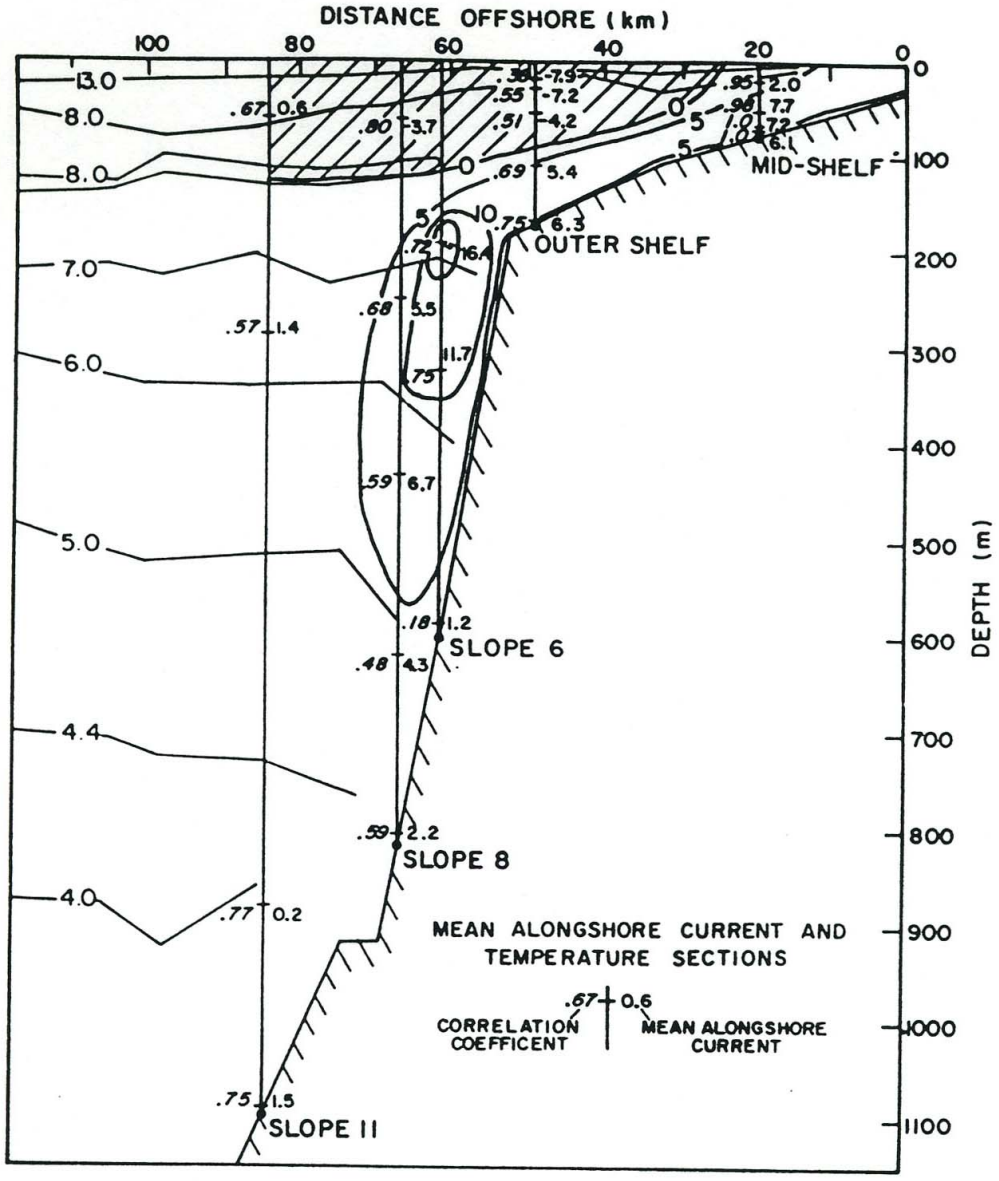

Figure 9: Along-shore currents off the U.S. West Coast (Hickey, 1979).

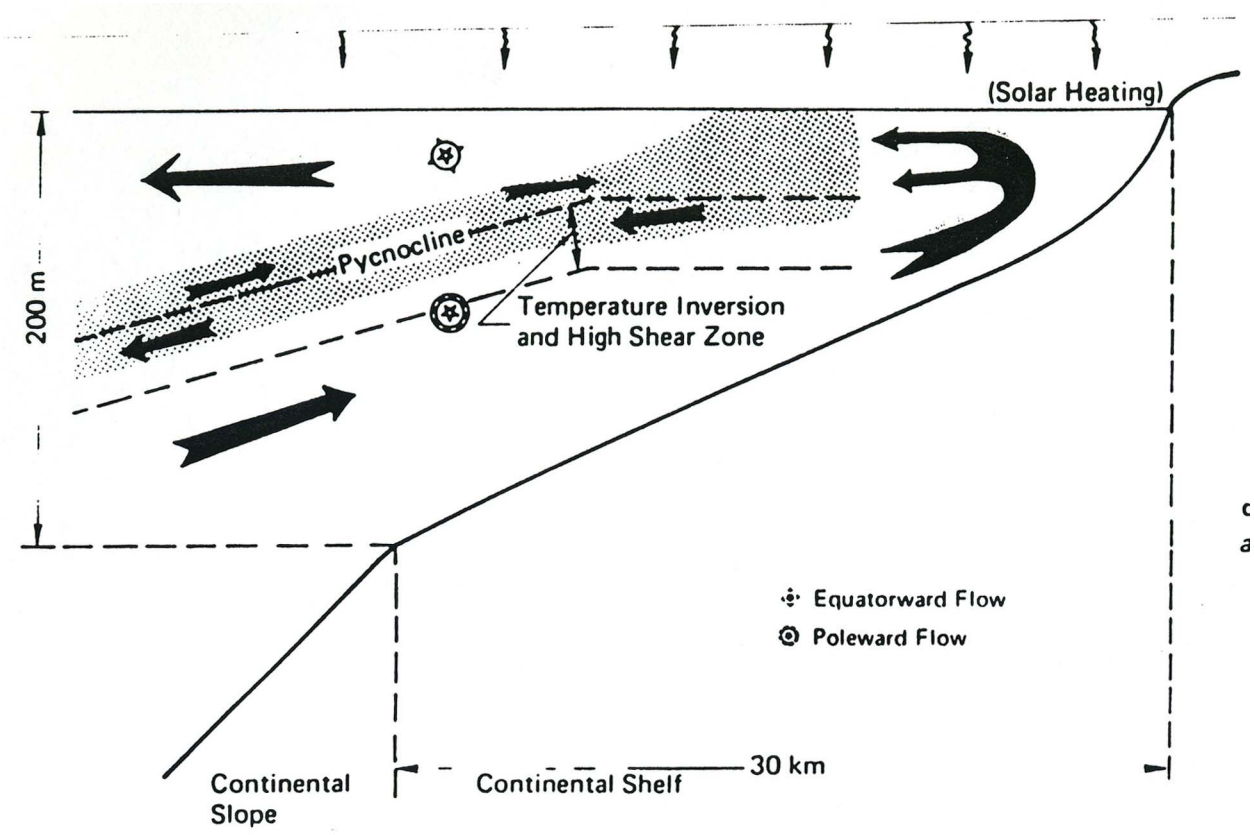

Figure 10: Sketch of upwelling circulation adjacent to an eastern boundary with equatorward winds (O'Brien, 1975).

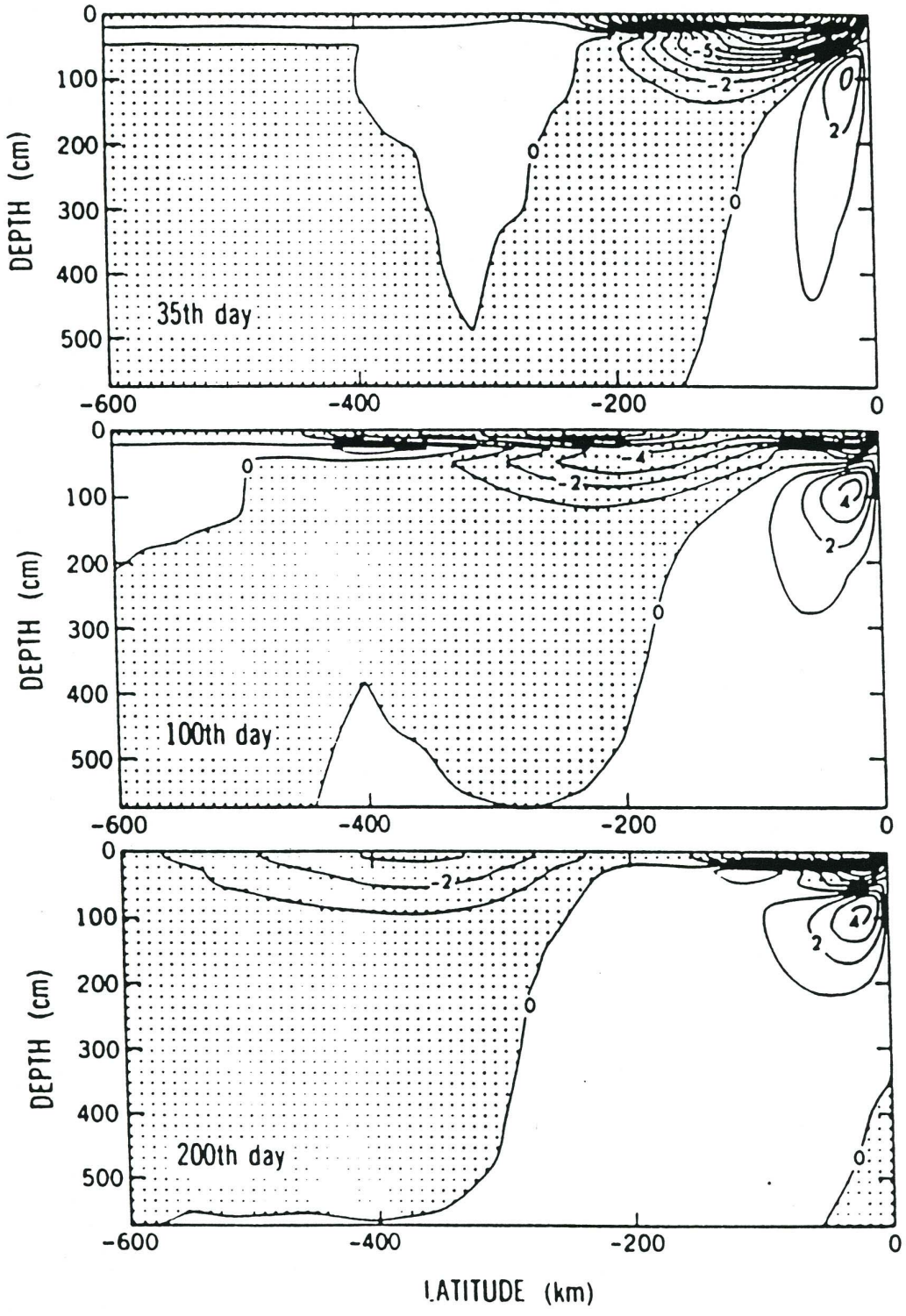

Figure 11: Modeled along-shore currents during an upwelling event (Philander and Yoon, 1982).

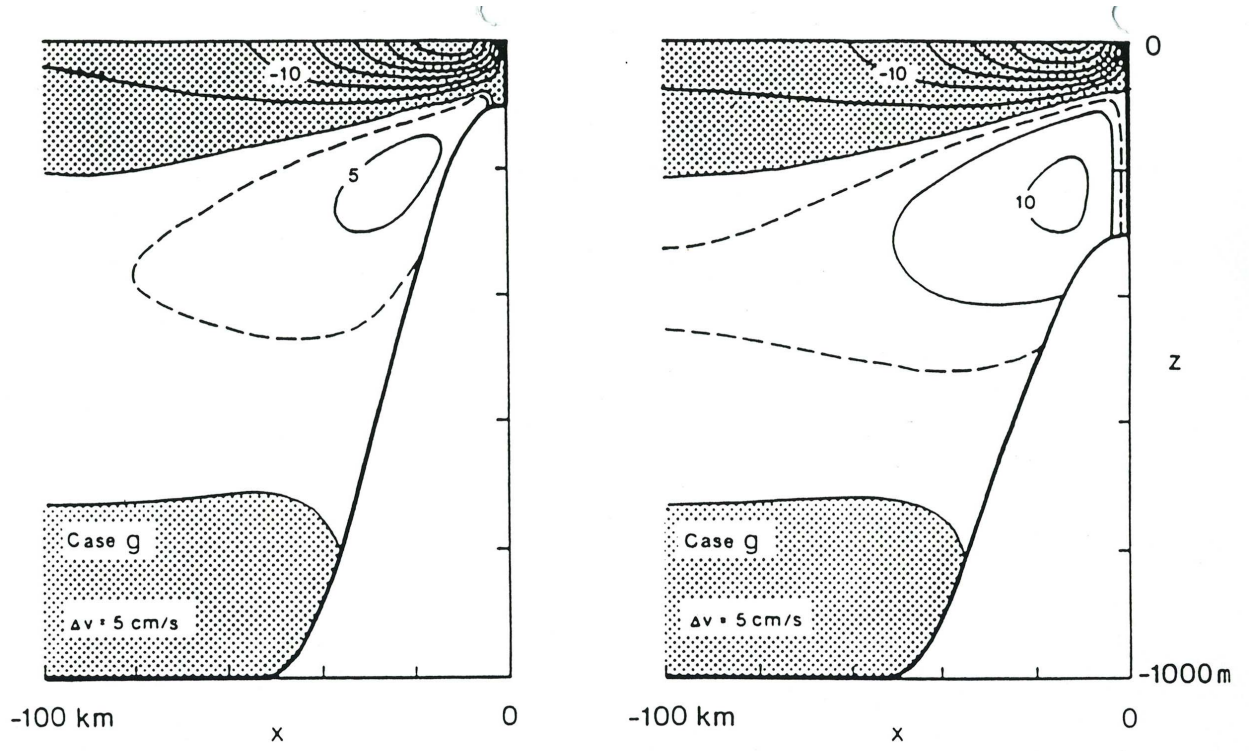

Figure 12: Modeled along-shore currents during an upwelling event over a shelf/slope topography (McCreary and Kundu, 1985).

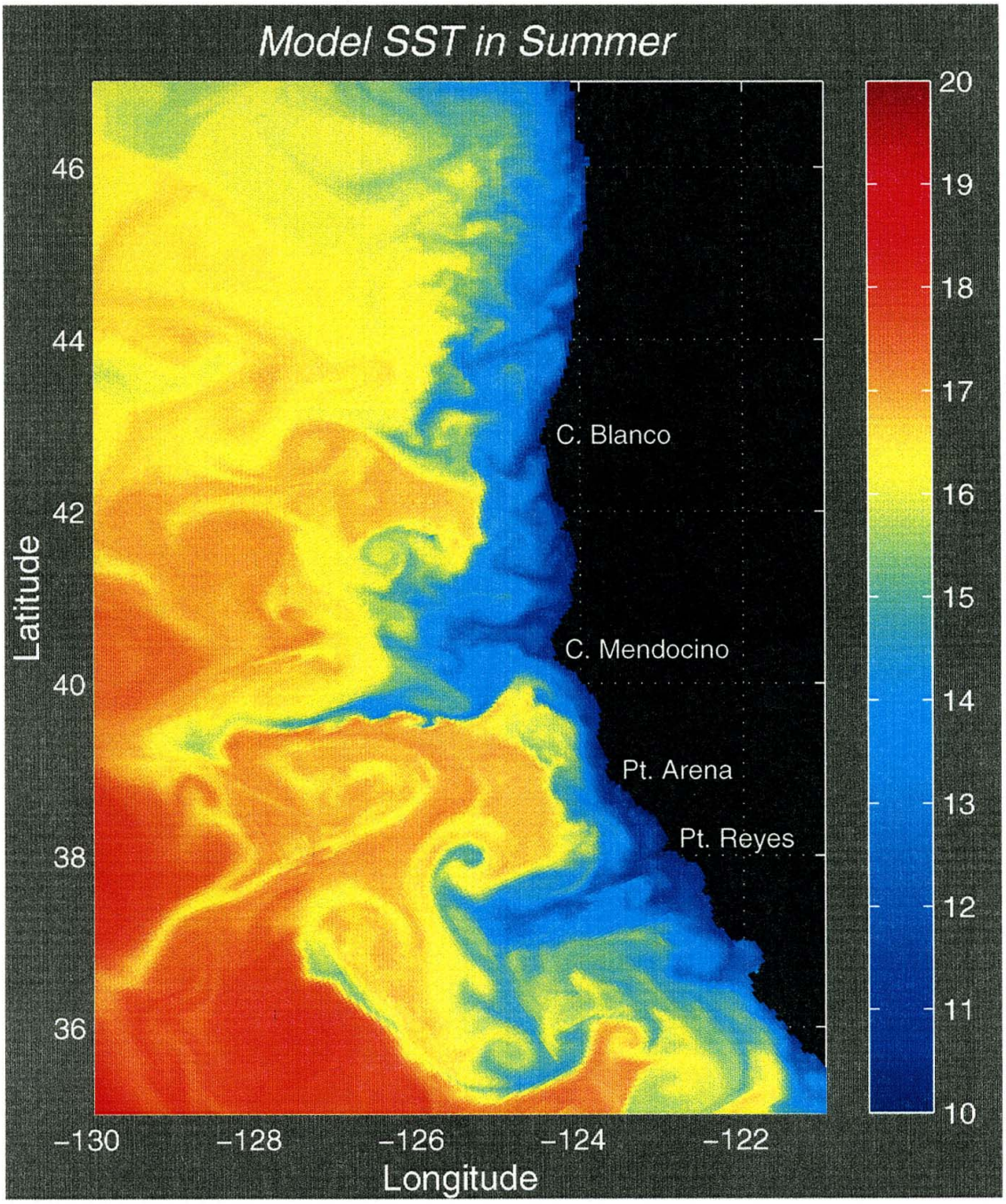

Figure 13: Instantaneous SST in a U.S. West Coast equilibrium model solution (Marchesiello et al., 2003).

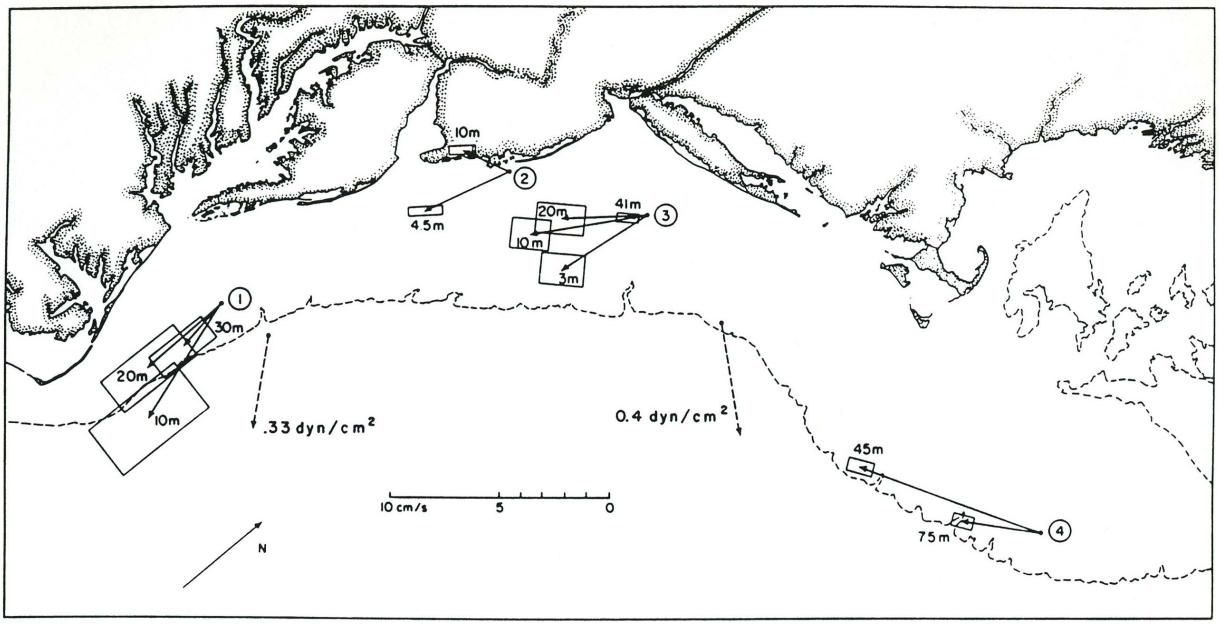

Figure 14: Mean currents in the Mid-Atlantic Bight (Beardsley and Boicourt, 1981).

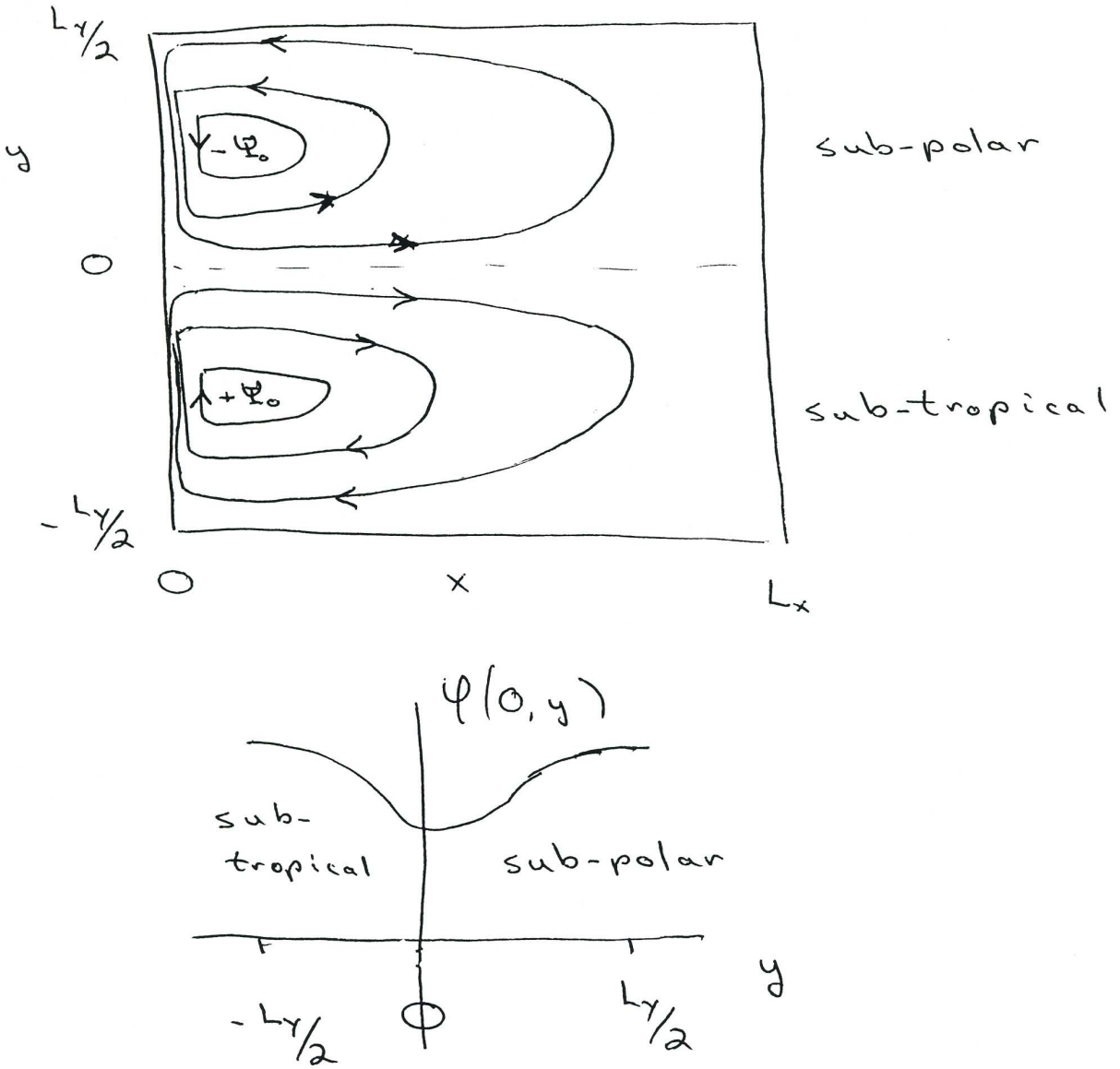

Figure 15: Barotropic pressure on the western boundary associated with a wind-driven double gyre, assuming a linear balance between horizontal flow and pressure.

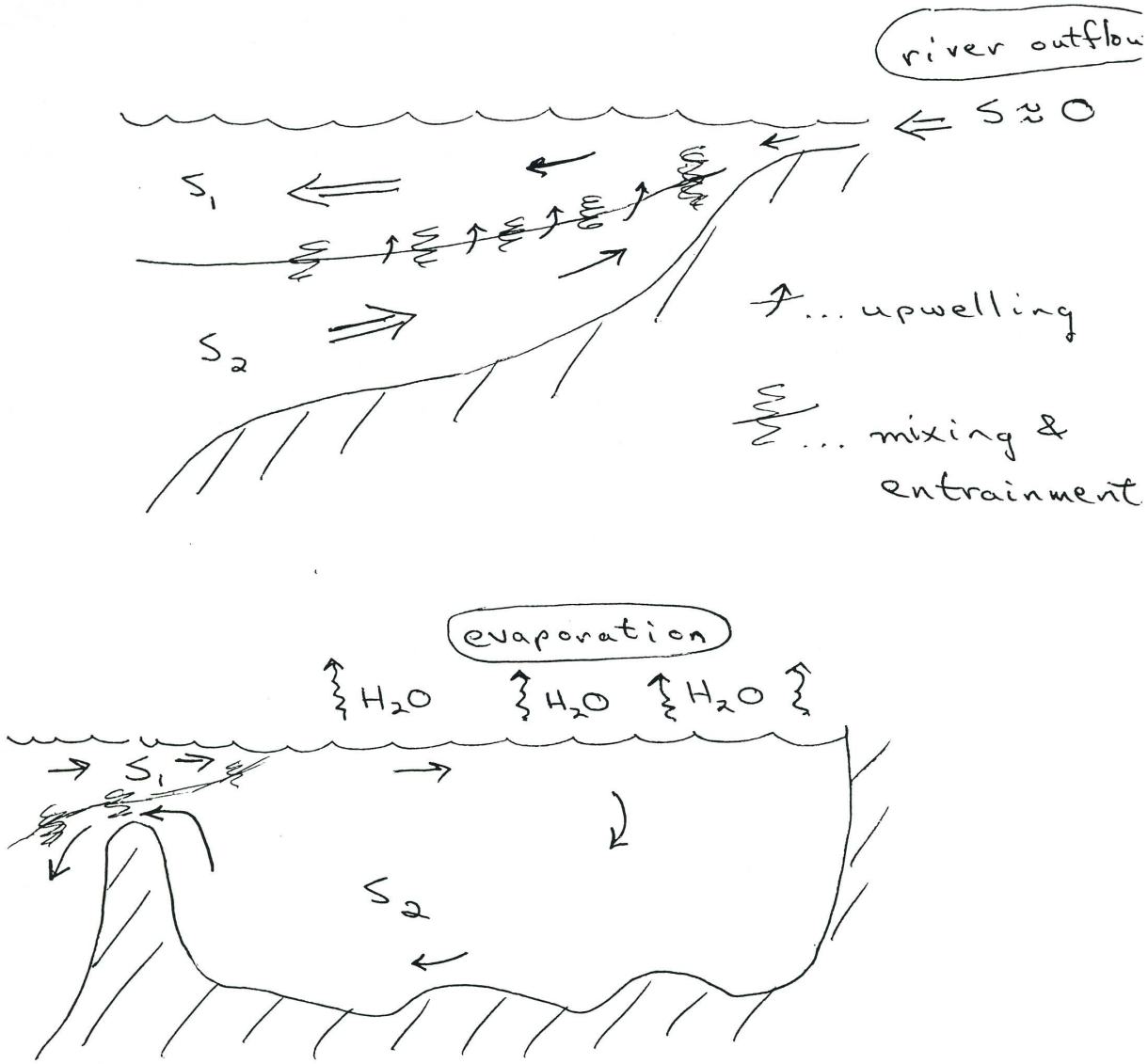

Figure 16: Sketch of estuarine circulations.

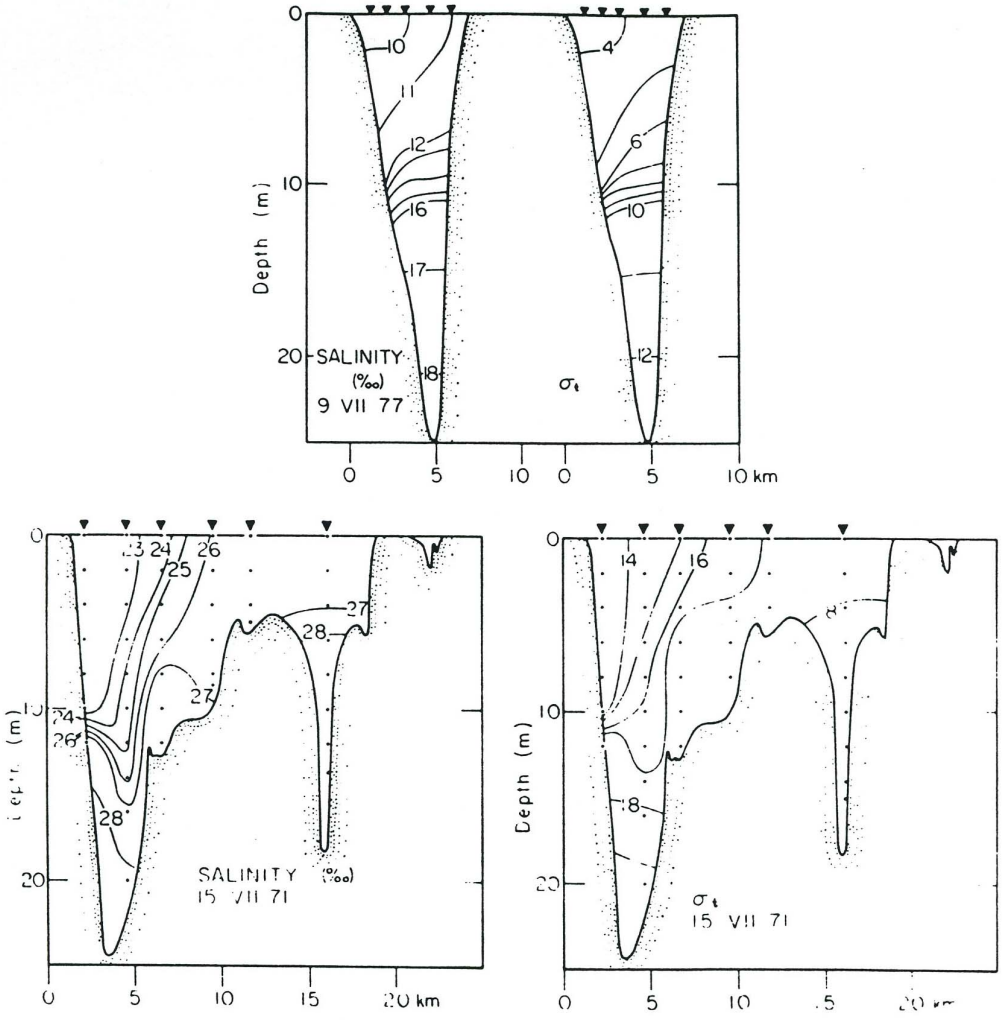

Figure 17: S and σ_t in Chesapeake Bay (Beardsley and Boicourt, 1981).

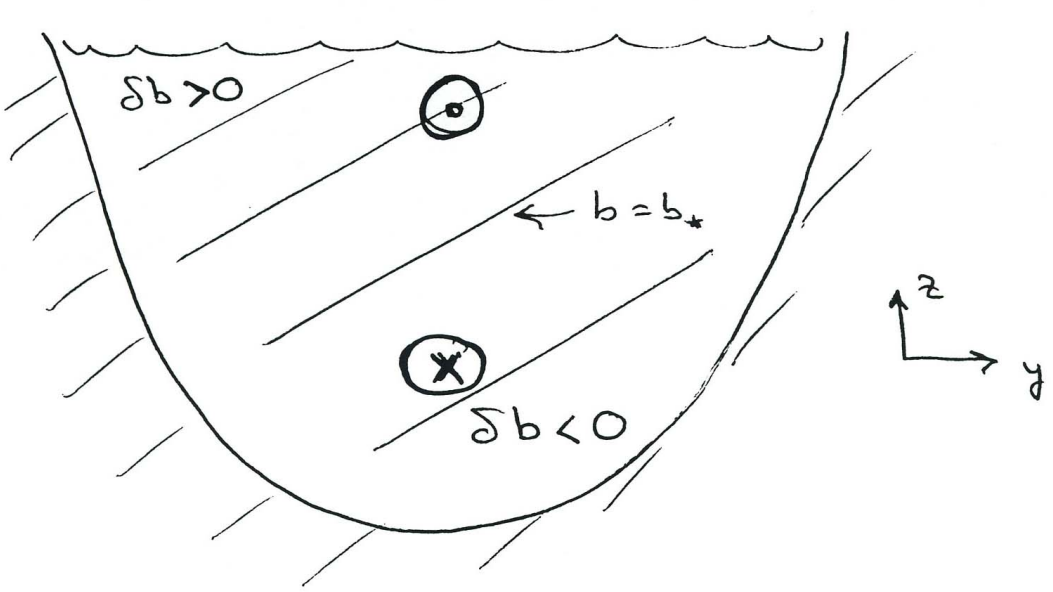

$$u_z = -\frac{1}{f}\phi_{yz}$$

$$= -\frac{1}{f} b_y$$

$$> 0$$

Figure 18: Sketch of isopycnal slopes in Chesapeake Bay.

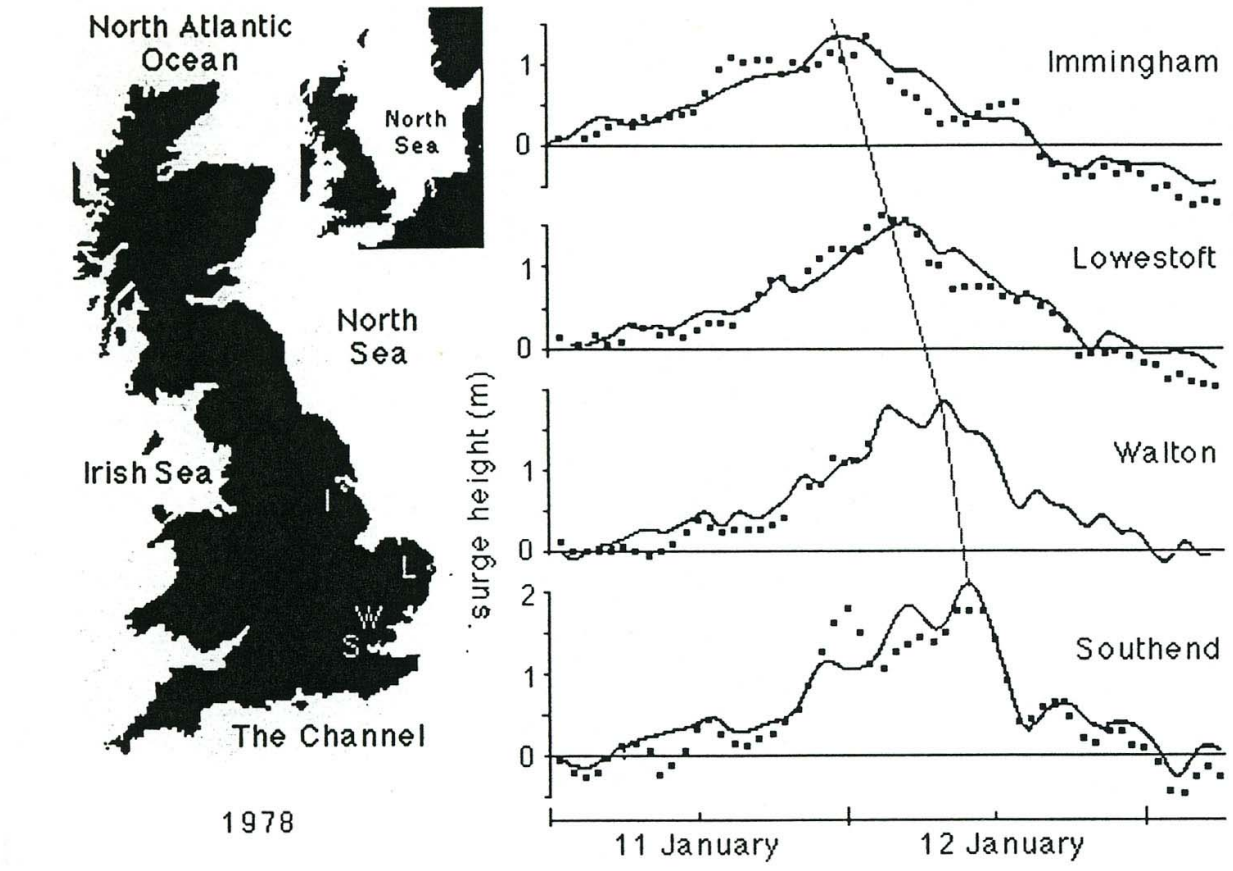

Figure 19: A storm surge in the North Sea (Tomczak, 1998).

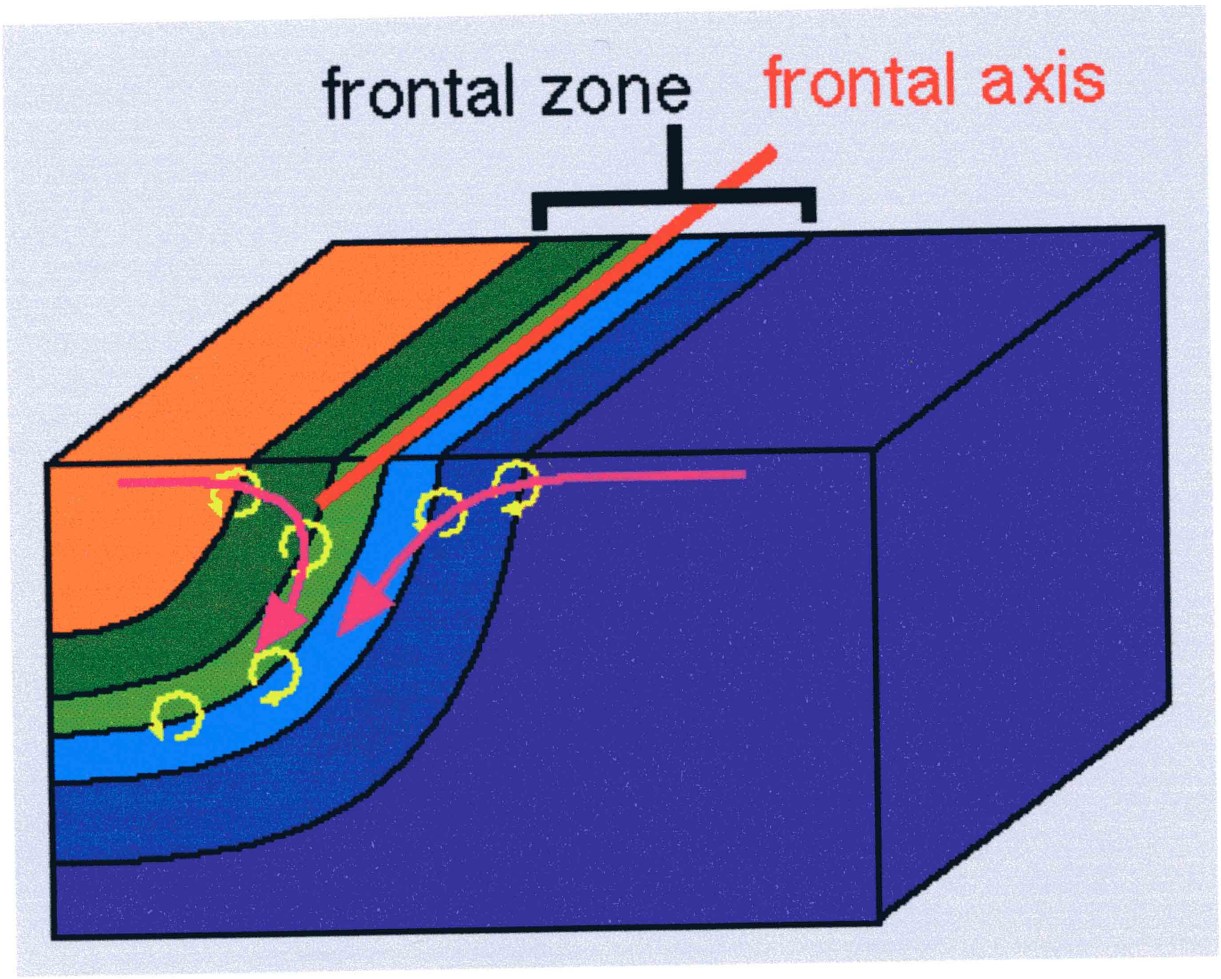

Figure 20: Sketch of T and circulation in a front formed by convergent flow at the surface (Tomczak, 1998).

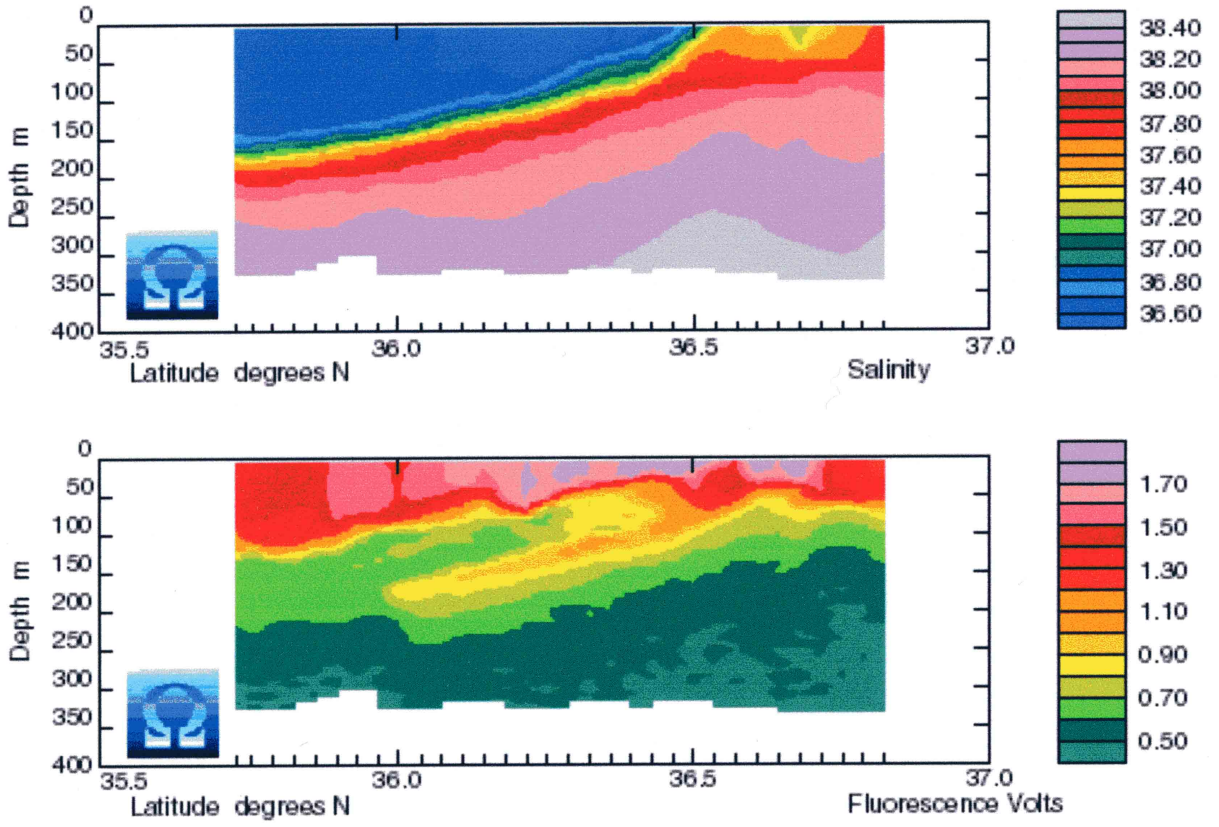

Figure 21: Evidence of downward movement in a Mediterranean front: upper panel is S and lower panel is flourescence (a measure of biological abundance). The downward water movement is much clearer in the latter field which does not contribute to the density stratification. (Tomczak, 1998).

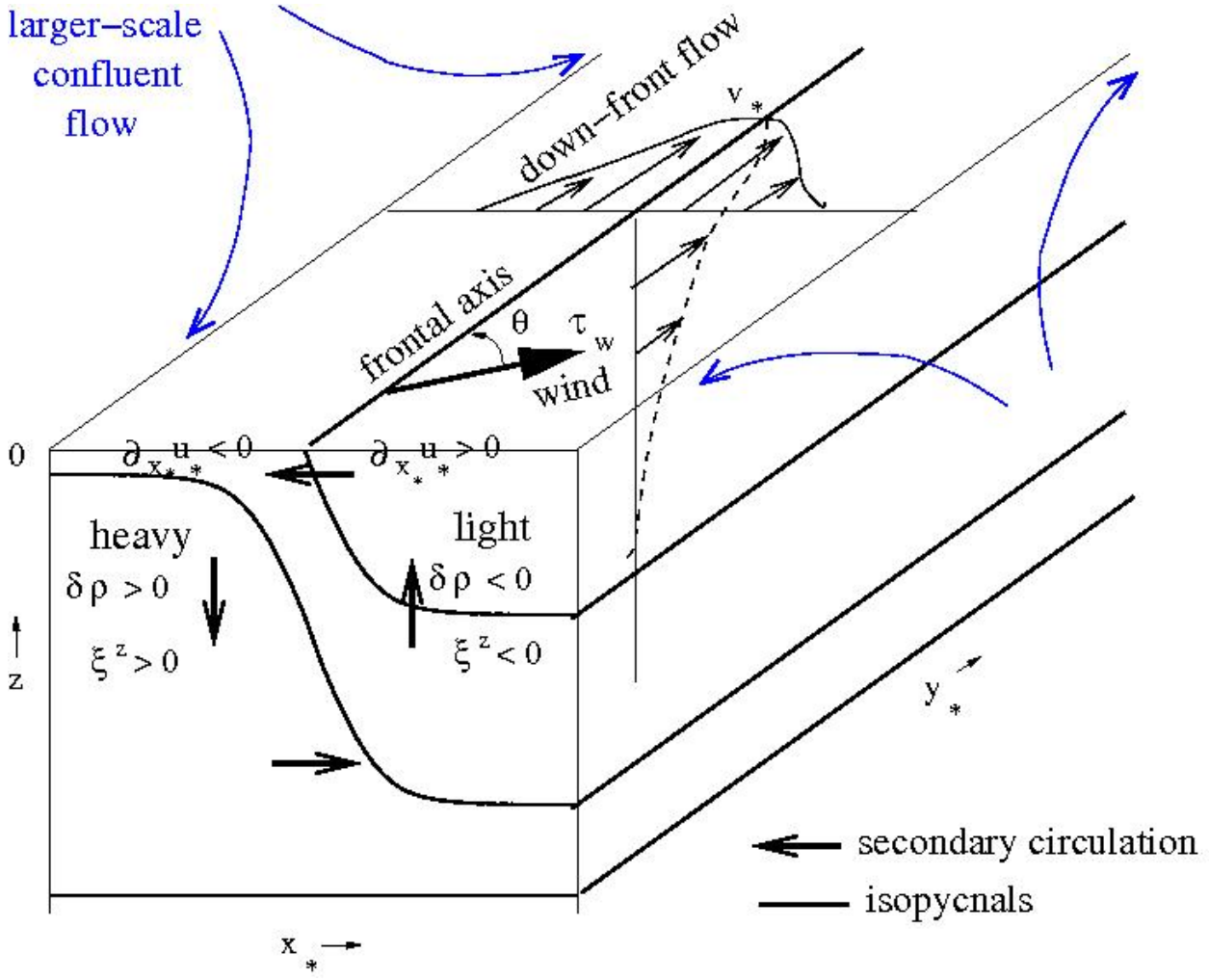

Figure 22: Sketch for an intensifying straight surface front with $f > 0$ in a larger-scale confluent flow (blue). (x_*, y_*) and (u_*, v_*) are rotated horizontal coordinates and velocity aligned with the frontal axis and its approximately geostrophic jet flow. $\delta\rho$ is the local potential density perturbation (Capet et al., 2007). Also shown is the orientation angle θ relative to the surface wind stress that can act to either intensify ($\theta = 0$) or abate ($\theta = \pi$) the rate of frontogenesis (Thomas and Lee, 2005).

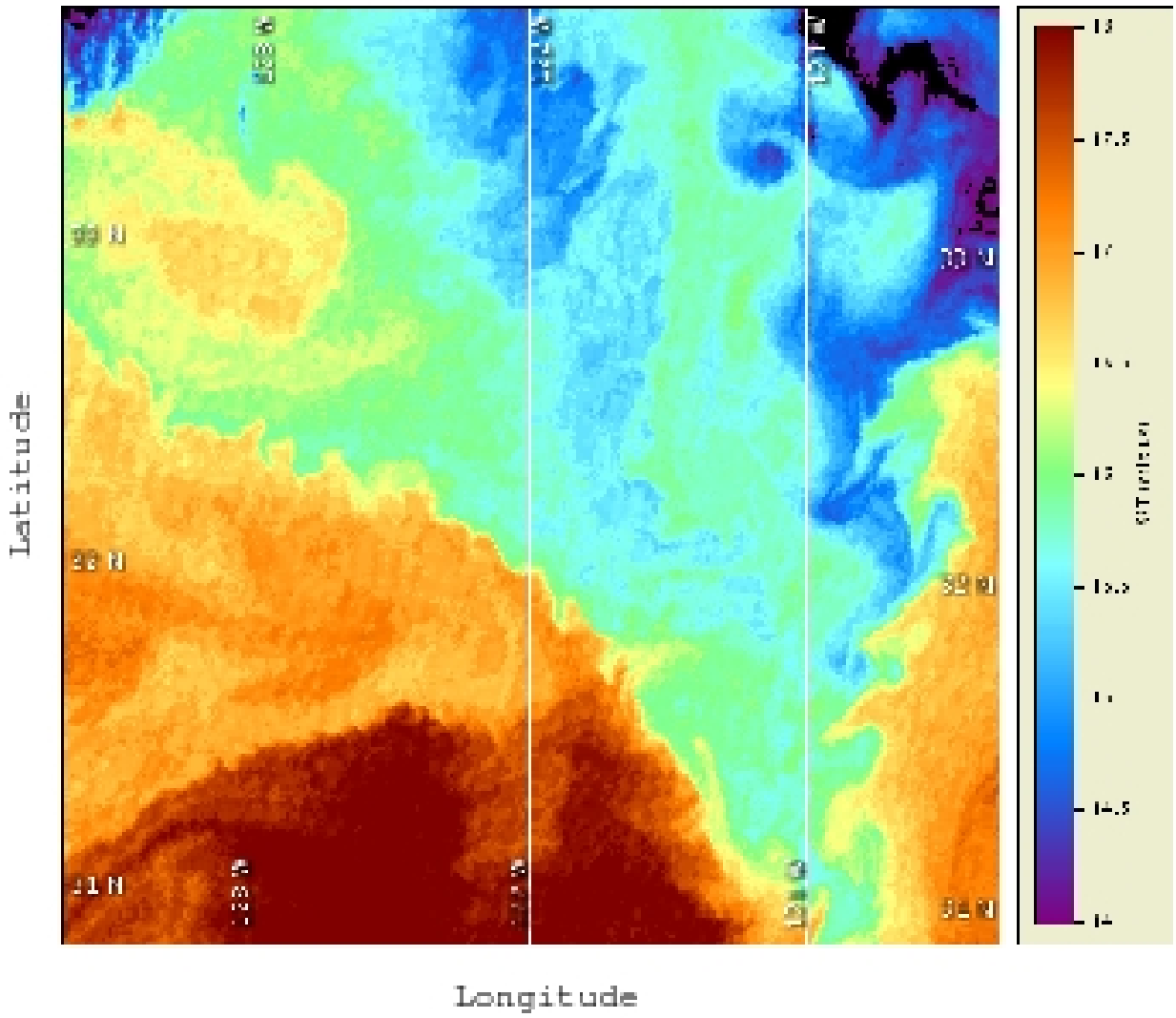

Figure 23: Sea surface temperature measured on 3 June 2006 off Point Conception in the California Current from COASTWATCH (`http://coastwatch.pfeg.noaa.gov/coastwatch/`). The fronts between recently upwelled water (*i.e.,* 15-16 ^{o}C) and off-shore water ($\geq$ 17 ^{o}C) show submesoscale instabilities with wavelengths around 30 km (right front) or 15 km (left front). Images for 1 d earlier and 4 d later show persistence of the instability events (Capet et al., 2007).

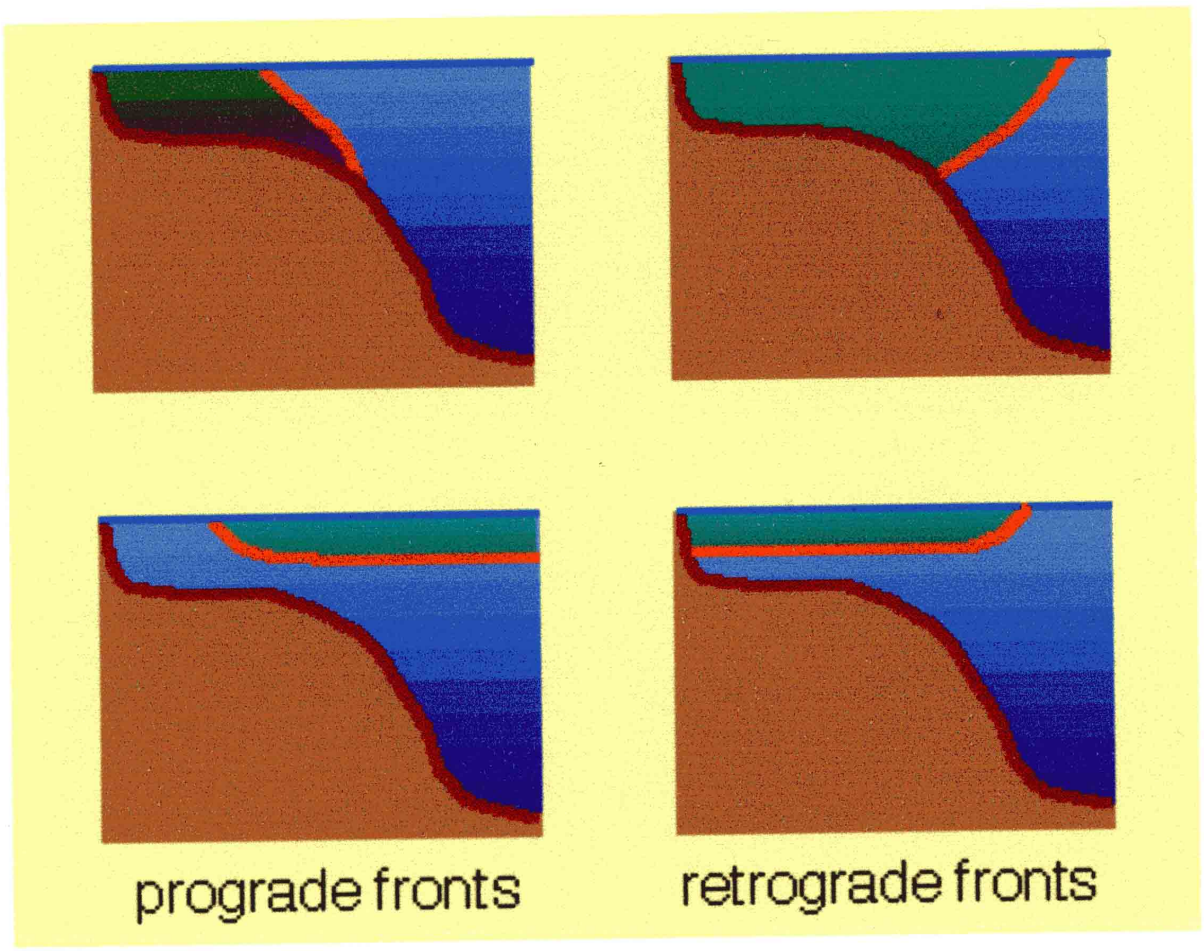

Figure 24: Sketch of prograde and retrograde fronts, distinguished by their orientation to the coastline and bottom slope (Tomczak, 1998).

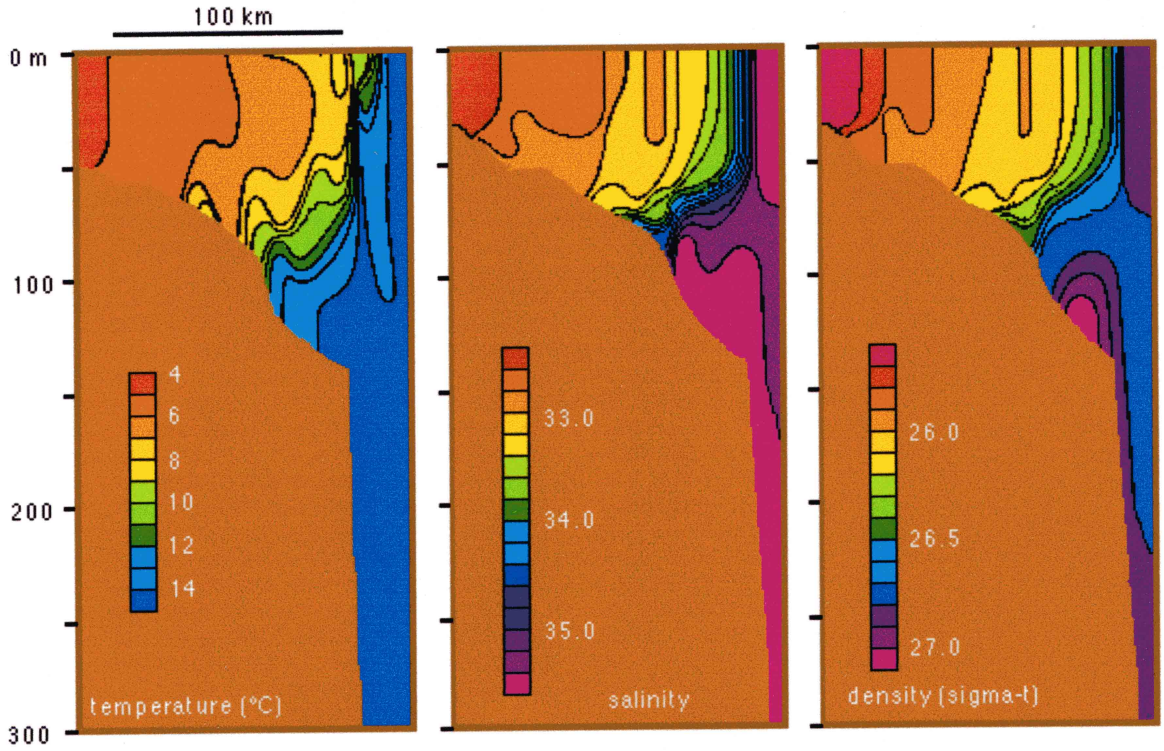

Figure 25: Hydrographic section through the shelf-break front in the Mid-Atlantic Bight, taken south of Rhode Island in April 1974 (Tomczak, 1998).

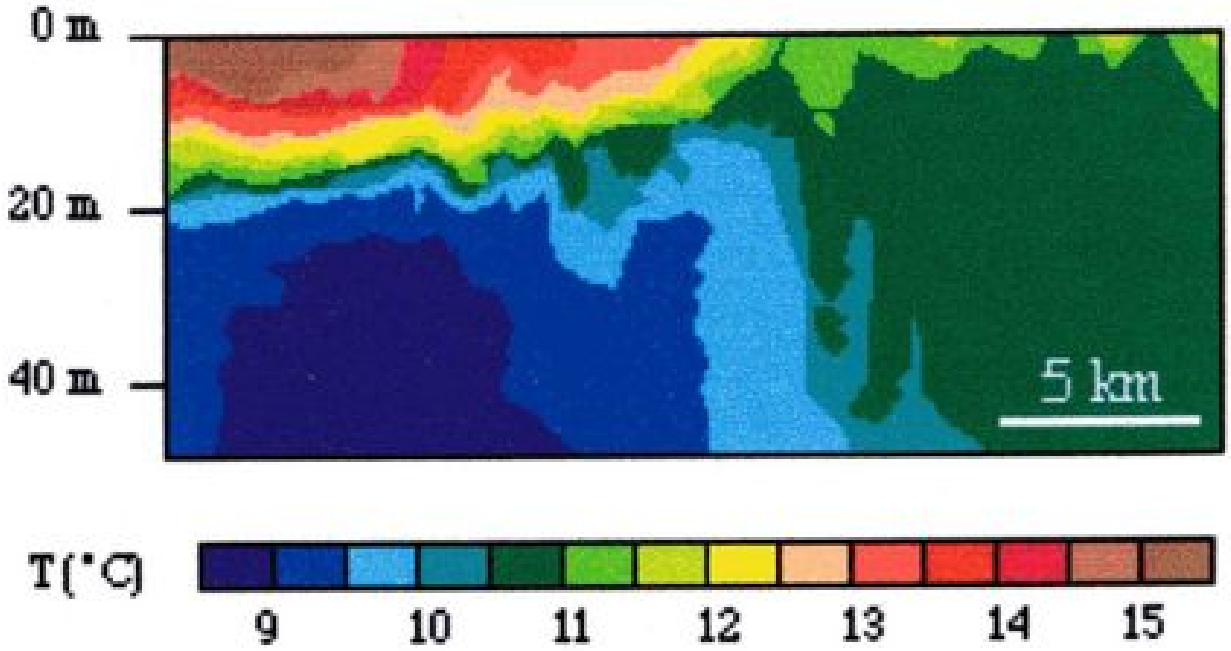

Figure 26: The observed T field in a shallow-water front in the Irish Sea, with deeper water to the left (Tomczak, 1998).

References

Allen, J.: 1980, Models of wind-driven currents on the continential shelf. *Ann. Rev. Fluid. Mech.*, **12**, 389–433.

Allen, J., L. Walstad, and P. Newberger: 1991, Dynamics of the coastal transition zone jet. 2. Nonlinear finite amplitude behavior. *J. Geophys. Res.*, **96**, 14995–15016.

Beardsley, R. and W. Boicourt: 1981, On estuarine and continental-shelf circulation in the middle atlantic bight. *Evolution of Physical Oceanography*, B. Warren and C. Wunsch, eds., MIT Press, 198–233.

Brink, K.: 1991, Coastal-trapped waves and wind-driven currents on the continental shelf. *Ann. Rev. Fluid. Mech.*, **23**, 389–412.

Capet, X., J. McWilliams, M. Molemaker, and A. Shchepetkin: 2007, Mesoscale to submesoscale transition in the California Current System: Frontal processes. *J. Phys. Ocean.*, in press.

Catelao, R., T. Mavor, J. Barth, and L. Breaker: 2006, Mesoscale to submesoscale transition in the California Current System: Frontal processes. *J. Geophys. Res.*, **111**, C09026.1–13.

Chen, C., R. Beardsley, and R. Limeburner: 1995, A numerical study of stratified tidal rectification over finite-amplitude banks. I: Symmetric banks. II: Georges Bank. *J. Phys. Ocean.*, **25**, 2090–2128.

Csanady, G.: 1982, *Circulation in the Coastal Ocean*. Reidel, 279 pp.

Denman, K. and M. Abbott: 1994, Time scales of pattern evolution from cross-spectrum analysis of avhrr and czcs imagery. *J. Geophys. Res.*, **99**, 7433–7442.

Harms, S. and C. Winant: 1998, Characteristic patterns of the circulation in the santa barbara channel. *J. Geophys. Res.*, **103**, 3041–3065.

Hickey, B.: 1979, The california current system. *Prog. Oceanog.*, **8**, 191–279.

Huyer, A., J. Barth, P. Kosro, R. Shearman, and R. Smith: 1998, Upper-ocean water mass characteristics of the california current, summer 1993. *Deep-Sea Res.*, **45**, 1411–1442.

Kelly, K., R. Beardsley, R. Limeburner, K. Brink, J. Paduan, and T. Chereskin: 1998, Variability of the near-surface eddy kinetic energy in the California Current based on altimetric, drifter, and moored current data. *J. Geophys. Res.*, **103**, 13,067–13,083.

LeBlond, P. and L. Mysak: 1978, *Waves in the Ocean*. Elsevier Press, 602 pp.

Longuet-Higgins, M.: 1968, The eigenfunctions of Laplace's tidal equations over a sphere. *Philos. Trans. R. Soc. London A*, **1132**, 511–607.

Marchesiello, P., J. McWilliams, and A. Shchepetkin: 2003, Equilibrium structure and dynamics of the California Current System. *J. Phys. Ocean.*, **33**, 753–783.

McCreary, J. and P. Kundu: 1985, Western boundary circulation driven by an alongshore wind with application to the Somali Current System. *J. Marine Res.*, **43**, 493–516.

O'Brien, J.: 1975, Models of coastal upwelling. *Numerical Models of Ocean Circulation*, R. Reid, ed., Nat. Acad. Sci. Press, 204–215.

Philander, S. and J. Yoon: 1982, Eastern boundary currents and coastal upwelling. *J. Phys. Ocean.*, **12**, 862–879.

Pierce, S., J. Allen, and L. Walstad: 1991, Dynamics of the coastal transition zone jet. *J. Geophys. Res.*, **96**, 14979–14993.

Stegmann, P. and F. Schwing: 2007, Demographics of mesoscale eddies in the California Current. *Geophys. Res. Lett.*, **34**, L14602 – 1–4.

Strub, P., P. Kosro, A. Huyer, and C. Collaborators: 1991, The nature of cold filaments in the California Current System. *J. Geophys. Res.*, **96**, 14743–14768.

Swenson, M. and P. Niiler: 1996, Statistical analysis of the surface circulation of the California Current. *101*, **101**, 22631–22645.

Thomas, L. and C. Lee: 2005, Intensification of ocean fronts by down-front winds. *J. Phys. Ocean.*, **35**, 1086–1102.

Tomczak, M.: 1998, *Shelf and Coastal Oceanography*. http://gyre.umeoce.maine.edu/physicalocean/Tomczak/index2.html.

Tomczak, M. and J. Godfrey: 2003, *Regional Oceanography: An Introduction*. Pergamon Press, 390 pp.